Microplasmas for nanomaterials synthesis

2010 J. Phys. D: Appl. Phys. 43 323001

(http://iopscience.iop.org/0022-3727/43/32/323001)

IOP PUBLISHING JOURNAL OF PHYSICS D: APPLIED PHYSICS

J. Phys. D: Appl. Phys. **43** (2010) 323001 (21pp) doi:10.1088/0022-3727/43/32/323001

TOPICAL REVIEW

Microplasmas for nanomaterials synthesis

Davide Mariotti[1,3] **and R Mohan Sankaran**[2,3]

[1] Nanotechnology and Advanced Materials Research Institute (NAMRI), University of Ulster, Newtownabbey, BT37 0QB, UK

[2] Department of Chemical Engineering, Case Western Reserve University, Cleveland, OH 44106, USA

E-mail: d.mariotti@ulster.ac.uk and mohan@case.edu

Received 4 May 2010, in final form 30 June 2010
Published 29 July 2010
Online at stacks.iop.org/JPhysD/43/323001

Abstract

Microplasmas have attracted a tremendous amount of interest from the plasma community because of their small physical size, stable operation at atmospheric pressure, non-thermal characteristics, high electron densities and non-Maxwellian electron energy distributions. These properties make microplasmas suitable for a wide range of materials applications, including the synthesis of nanomaterials. Research has shown that vapour-phase precursors can be injected into a microplasma to homogeneously nucleate nanoparticles in the gas phase. Alternatively, microplasmas have been used to evaporate solid electrodes and form metal or metal-oxide nanostructures of various composition and morphology. Microplasmas have also been coupled with liquids to directly reduce aqueous metal salts and produce colloidal dispersions of nanoparticles. This topical review discusses the unique features of microplasmas that make them advantageous for nanomaterials synthesis, gives an overview of the diverse approaches previously reported in the literature and looks ahead to the potential for scale-up of current microplasma-based processes.

(Some figures in this article are in colour only in the electronic version)

1. Introduction

Microscale plasmas are a special class of electrical discharges formed in geometries where at least one dimension is reduced to sub-millimetre length scales [1]. As a result of their pD (where p is pressure and D is the smallest physical dimension) scaling, 'microplasmas' have been found to be uniquely characterized by high-pressure stability [2], non-equilibrium thermodynamics [3, 4], non-Maxwellian electron energy distribution functions (EEDFs) [5], high electron densities [4], excimer generation [6–8] and new sheath dynamics [9]. Overall, these properties differentiate microplasmas from other high-pressure sources such as arcs, coronas and DBDs, although in the case of the latter, filamentary microdischarges are formed within the plasma volume. As a result, there has been intense interest in the scientific community to develop and implement microplasmas in a variety of different venues.

The salient features of microplasmas, both in terms of discharge physics and operating regime, are especially conducive to materials applications. The existence of significant populations of energetic electrons (i.e. 10 eV or higher) allows efficient, non-thermal dissociation of molecular gases or other vapour precursors to produce high concentrations of reactive radical species [10]. Whereas low-pressure plasmas entail a large cost due to the equipment and maintenance of the reactors, operation near or at atmospheric pressure is cheaper, easier to implement and highly desirable for industrial applications [11]. Because of their small size, microplasmas are capable of locally etching or sputtering films and substrates to directly create microscale patterns without the need for photolithography [12–22]. Their versatility has led to the development of microjets or microsprays for thin film deposition and coating applications [23–37]. Parallel operation has also been demonstrated as a potential route to perform combinatorial experiments for materials optimization [38].

A related but new direction for microplasma technology is the synthesis of nanoscale materials or nanomaterials (defined as materials with at least one dimension less

[3] Authors to whom any correspondence should be addressed.

than 100 nm). Because of current limitations associated with conventional top-down approaches which combine plasmas with photolithography to define the dimensionality of materials, nanomaterials must be prepared from the bottom up by dissociating molecular precursors and nucleating from atomic (or polyatomic) constituents. While wet chemical methods are more common and well known, plasma-based processes have also been previously used for this purpose and are characterized by higher purity, compatibility with solid-state device manufacturing and non-specific chemistry so that a wide range of nanomaterials are possible including group II–VI, III–V and IV semiconductors, noble and transition metals and insulators such as metal oxides or polymers. Additionally, as described in recent reviews [39–41], low temperature plasmas create a unique environment for nanomaterial synthesis that limits agglomeration and enables the formation of crystalline materials by selective heating. Microplasmas offer many of these same benefits, but also open up new possibilities for nanomaterials synthesis, functionalization and assembly. In comparison with low-pressure, large-scale plasmas, the following are some key advantages of microplasma-based processes for nanomaterials synthesis:

(1) *High-pressure chemistry.* The mechanism for nucleation in a reactive plasma has been surmised to involve gas-phase collisions between radical moieties; an illustrative example is the nucleation of Si clusters from Si_xH_y radicals in a silane plasma [42]. At higher pressures (hundreds of torr or higher), these collisions are significantly enhanced, leading to highly favourable conditions for particle formation (as opposed to film deposition) [43]. Since microplasmas are operated at atmospheric pressure *and* contain high radical densities, particle nucleation from radical polymerization should be far more efficient than low-pressure plasma systems.

(2) *Continuous-flow.* While conventional low-pressure plasmas have been used to form nanoparticles, in these batch-type processes, particles can nucleate, grow and eventually agglomerate due to the long residence times [44]. It is therefore difficult to sufficiently control growth and synthesize well-defined materials in terms of size, shape, composition, etc. Collecting material is also a challenge because of electrostatic trapping and deposition on the electrodes. Coupling gas flow to a plasma to create a continuous-flow reactor, as in the case of microplasma jets, effectively addresses these issues. Vapour precursors flow into the plasma volume to nucleate material, followed by quenching of the growth and rapid flow out of the reactor volume. Because the process is usually conducted at steady state, the residence time can be varied to tune the mean particle size *in a single step*, with minimal dispersity and agglomeration [45]. High yields of material are easily obtained by filtration or thin film deposition of the aerosol product.

(3) *Microreactor geometry.* A critical issue for nanoparticle growth is the reactor residence time which will have a characteristic distribution and, thus, almost always result in non-uniform particle nucleation and growth. A simple approach to controlling the residence time distribution (RTD) is to reduce the reactor volume. As demonstrated for liquid-phase systems, microscale reactors, characterized by short residence times in the milli- to microsecond range, can produce highly uniform nanomaterials because temperature and concentration variations are minimized and the RTD is narrowed [46]. A similar effect is expected for continuous-flow microplasma jets since their reactor volume is often on the order of nanolitres[4] and with flow rates in the 100 sccm range, residence times can easily approach 1 μs. There are other benefits as well associated with a microreactor geometry including reduced consumption of precursors, lower safety-related risk and the potential for scale-up by operating in parallel.

(4) *Self-assembly/organization.* In a plasma environment, nanoparticles can acquire charge and interact with one another through Coulombic and van der Waals forces to form self-organized structures. Atmospheric-pressure microplasmas have been shown to produce similar effects and promote the self-organization of nanoparticles [47, 48]. These preliminary results hint at the exciting possibility of guiding the formation of large-scale, ordered nanostructures through a microplasma-based process.

For these reasons, microplasmas are expected to have a significant impact on the synthesis and applications of nanomaterials. In this review, we summarize recent progress in the field with the hope of bringing into focus existing and future directions for this exciting area of research. We begin in section 2 by discussing the novel physical properties of microplasmas that motivate their use for nanomaterials synthesis. In section 3, we present examples of recent work including nanoparticle synthesis, catalytic growth of 1D nanomaterials, thin film deposition of ordered nanostructures and liquid applications. In section 4, we explore some of the fundamental and technological challenges related to nanomaterials synthesis that must be overcome for microplasmas to find widespread use in commercial applications. We conclude with a brief outlook for future directions in section 5.

2. Physics of microplasma sources

Since the first reports of microplasma sources, there has been a significant amount of interest in characterizing and understanding the unique properties of plasmas at new length scales. An analogy could be made with the field of nanotechnology as both are motivated by exploiting confinement for useful purposes, albeit at different dimensions. In both cases, as the physical boundaries are reduced, the properties of the 'material' change. For solid-state materials, this is evident below dimensions of ~10–100 nm, depending

[4] A simple calculation for the volume of a cylindrically shaped microplasma jet with a diameter of 200 μm and a length of 2 mm yields a volume of 30 nL. This approximation may be too small, if the plasma expands outside our idealized cylinder geometry, or too large if the plasma is constricted by flow or electric field effects.

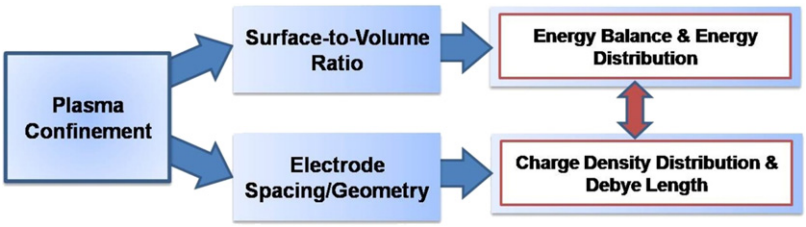

Figure 1. Conceptual diagram of the influence of plasma confinement on energy balance and plasma dynamics.

on the material and the property under observation. For instance, while the melting temperature of bulk gold is approximately 1064 °C, this value is drastically reduced and depends inversely on size for Au nanoparticles less than 10 nm in diameter [49].

Similarly, it might be expected that confining plasmas to small dimensions will result in new physical behaviour. At some critical size, a transition from a plasma with bulk properties to a new phase with size-dependent properties must occur. Two general parameters that may determine this transition are the *surface-to-volume ratio* and the *electrode spacing* (see figure 1). The surface-to-volume ratio, which increases as the size of the plasma decreases, will alter the overall energy balance and could lead to plasma stability (or instability) within different regions of the operating parameter space. Decreasing the electrode spacing will change the electric field distribution and, thus, impact the charge distribution and overall plasma neutrality. Overall, these effects should have strong implications on the energy distribution of the different species (electrons, ions, radicals, neutrals) and on the physical structure of the plasma, either simultaneously or independently. There is now significant evidence in the literature that a transition takes place when the dimensions of the plasma are reduced to the micrometre scale, and a large number report noticeable differences at sub-millimetre scales [50–53]. Traditional properties and scaling laws for plasmas do not hold at these dimensions, justifying the existence of a different regime of operation, hereafter referred to as the microplasma regime (MPR). There is also recent evidence that other transitions might occur when plasmas are confined to even smaller scales [54].

The definition of microplasmas as plasmas confined within sub-millimetre cavities in at least one dimension is finding large consensus in the literature [9, 50, 52, 53, 55–62] and is at least partially motivated by the existence of a new physical regime. Although this remains an operational definition, which indicates our limited understanding, there have been many experimental and theoretical efforts to study this regime. In the following section, we provide a brief summary of recent work aimed at elucidating the physics and operation of microplasmas.

2.1. Energy balance and charge neutrality

A number of interesting experimental and theoretical results related to fundamental characterization of microplasmas have been reported in recent years, underpinned by basic energy balances and extrapolations from traditional plasma parameters. One important aspect that must be considered for nanomaterials synthesis is how to control the energy flow which will determine the transition from a non-equilibrium (i.e. low temperature) to equilibrium (i.e. thermal) plasma. Non-equilibrium plasmas are more desirable for materials synthesis because of the possibility of opening chemical pathways that may not be possible by thermal means. In addition, low temperature processes allow temperature-sensitive materials to be used. Simple energy considerations can show that reducing the plasma volume affects the overall energy flow, as determined by zero-dimensional (0D) energy balance equations. In general, confinement causes a simultaneous increase in electron temperature and electron density [63]. Electrons gain energy as a result of stronger electric fields and exchange energy through collisions with other species (i.e. neutrals, ions, etc) [51]. The energy balance is then determined by the electron density and the effective rate of energy exchange through inelastic collisions (e.g. vibrational–rotational energy exchange). The collision frequency for heating of neutral atoms or molecules, υ_{heat}, can be expressed as the following:

$$\upsilon_{\mathrm{heat}} = n_{\mathrm{e}} K_{\mathrm{e}}(T_{\mathrm{e}}), \tag{1}$$

where n_{e} is the electron density, K_{e} is the collision rate and T_{e} is an effective electron temperature (see below for more details on the definition of effective electron temperature). During each collision, an average energy (ε) is exchanged and the power density (P_{heat}/V) transferred as thermal energy can be written as

$$\frac{P_{\mathrm{heat}}}{V} = \varepsilon(T_{\mathrm{e}}) n_{\mathrm{g}} n_{\mathrm{e}} K_{\mathrm{e}}(T_{\mathrm{e}}), \tag{2}$$

where n_{g} is the gas density. In addition, we must consider the power loss (P_{cool}) per unit volume [64]:

$$\frac{P_{\mathrm{cool}}}{V} = n_{\mathrm{g}} C_{\mathrm{pl}} (T_{\mathrm{g}} - T_0) \nu_{\mathrm{hr}}, \tag{3}$$

where T_{g} is the temperature of the neutral gas atoms or molecules and T_0 is the wall temperature, ν_{hr} is the frequency of heat removal and C_{pl} is the heat capacity of the plasma. Assuming that heat conduction is the dominant cooling mechanism, equation (3) can be expressed as a function of parameters that are easier to measure [64]:

$$\frac{P_{\mathrm{cool}}}{V} \propto n_{\mathrm{g}} \frac{T_{\mathrm{g}}^{3/2}}{pD^2}, \tag{4}$$

where, as before, D is a parameter that refers to the size of a microplasma in one dimension and p is the pressure [65–68].

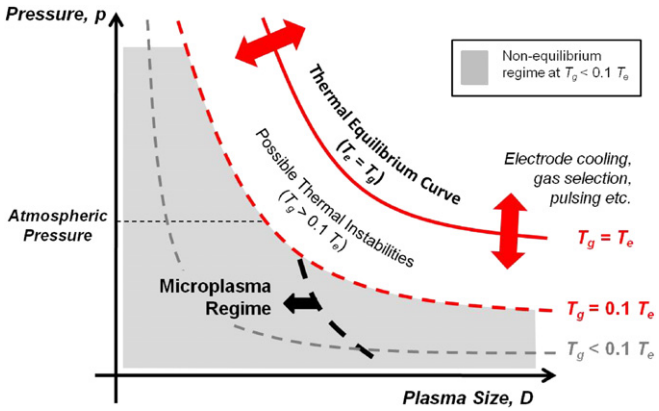

Figure 2. Regimes of plasma operation as a function of the pressure (p) and its physical size in one dimension (D). The transition from non-equilibrium to thermal equilibrium is indicated by the solid or dashed lines.

For a plasma at steady state (i.e. no gas flow), the power transferred to the gas must be equal to the power lost through conduction; therefore, we can relate equations (1) to (3) and obtain the following relationship:

$$D^2 \propto \frac{T_g^{3/2}}{p\varepsilon n_e K_e} \quad \text{or} \quad p \propto \frac{T_g^{3/2}}{D^2 \varepsilon n_e K_e} \tag{5}$$

The terms K_e and ε are generally a function of the EEDF. A complete analysis that takes into account the actual EEDF would be quite complicated considering that for microplasmas, the EEDF is non-Maxwellian (similarly to other high-pressure plasmas) and an extended high-energy tail exists [5, 69, 70]. Nonetheless, in the range of electron energies considered here, both K_e and ε can be shown to increase with the average electron energy or the effective electron temperature. The effective electron temperature, T_e, is useful when dealing with non-Maxwellian electron energy distributions [71, 78] and as a measure of the EEDF, we could now generally say that K_e and ε increase monotonically with T_e, at a slower rate for lower effective electron temperatures and more rapidly as inelastic collisions become more significant at higher effective electron temperatures. Hereafter, the word '*effective*' will be omitted with the implicit understanding that microplasmas are characterized by an unknown energy distribution for the electrons [51, 71].

The relationships found in equation (5) can be used for a basic analysis of the effect of confinement on plasmas. In figure 2, the pressure (p) is plotted as a function of the dimension of a plasma (D) where the thermal equilibrium limit (i.e. $T_e = T_g$) is indicated by the red curve; the non-equilibrium regime ($T_e > T_g$) is the area below the red curve indicated in grey. Near the thermal equilibrium curve, defined as the range of $T_g = 0.1T_e$ to $T_e = T_g$ [64], the plasma is likely to undergo thermal instabilities. Detailed discussion of the boundary between the MPR and bulk plasmas (black broken curve in figure 2) will be given in the next section; we first focus on the factors that define non-equilibrium conditions versus thermal conditions, with respect to the plasma size.

We emphasize that figure 2 is representative of a given input power, electrode geometry, gas composition, gas flow rate, etc. Thus, by modifying the configuration, operating conditions or the plasma system, the thermal curve is shifted and it is possible to achieve non-equilibrium within a range of volume–pressure combinations. In fact, a number of approaches have been used to maintain non-equilibrium conditions (see red double arrows in figure 2). Generally, these approaches impact either the frequency of heat removal term (e.g. electrode cooling [72, 73], convective gas flow [74]) or the K_e and ε terms (e.g. gas composition [15], barrier discharges [18], pulsed power [19]). For example, if the input power is increased, the thermal curve in figure 2 would shift down and to the left, resulting in a smaller non-equilibrium region, as expected for plasmas operated at higher powers. On the other hand, when electrodes are water-cooled, the frequency of heat removal, ν_{hr}, is enhanced (see equation (3)), and the pressure at which thermal equilibrium is reached (see equation (5)) is shifted to a higher value. Similarly, other techniques that are used to cool a plasma, such as gas flow, will cause the thermal curve to shift up and to the right. Thus, external cooling permits a non-equilibrium plasma to be maintained at atmospheric pressure and large volume.

The gas composition also affects the range of volume–pressure conditions where non-equilibrium characteristics can be sustained. Comparison of discharges formed in He and Ar is illustrative of the role of gas composition on these properties. Helium has been commonly used as the supply gas to produce non-equilibrium, large volume plasmas at atmospheric pressure [75]. Although the ionization energy for He is relatively high (24.6 eV), the minimum energy required for electron-induced excitation of He gas atoms (>21.2 eV) is similar. As a result, electrons transfer their energy effectively via ionization processes, allowing He plasmas to be ignited and sustained at relatively low power. As previously mentioned, lower powers shift the thermal equilibrium curve in figure 2 up and to the right, resulting in a larger window for non-equilibrium operation at atmospheric pressure, in agreement with previous experiments in He. In comparison, Ar is characterized by a larger difference between the lowest electron-induced excitation (>11.5 eV) and the ionization energy (15.8 eV) and excitation of Ar metastables can play a significant role in energy consumption. Consequently, a larger fraction of electrons are involved in inelastic collisions that do not contribute to ionization and higher power is required to sustain an Ar plasma. Therefore, the thermal equilibrium curve for Ar plasmas is shifted down and to the left and non-equilibrium operation at atmospheric pressure requires that the discharge volume is reduced. Other gas compositions, including molecular gases which may be of greater importance for materials applications, will be characterized by an even smaller non-equilibrium region since the energy of the electrons will be reduced by additional collisional pathways.

Let us now consider plasmas that are not confined to sub-millimetre dimensions, i.e. bulk plasmas. These large-scale, low-pressure plasmas with a characteristic electron temperature much higher than the gas temperature are

identified by a point in the *pD* space that lies within the grey area of figure 2, to the right of the MPR. If now the pressure is increased, the point moves up and, eventually, a state of thermal equilibrium is reached. This is verified by equation (5) where the consequence of increasing pressure is either plasma extinction, due to a decreasing electron temperature (which decreases K_e and ε) and/or decreasing electron density, or thermal equilibrium, whereby the electron temperature and gas temperature approach one another [52, 76]. It follows that in order to maintain non-equilibrium at atmospheric pressure, the volume of the plasma must be reduced (note that it has been observed experimentally that non-equilibrium characteristics are readily achieved at atmospheric pressure for sub-millimetre plasmas [52, 63]). As indicated by equation (5), reducing the size of a plasma at constant pressure (i.e. moving left from our starting point along the x-axis) results in a decrease in the gas temperature and/or an increase in the electron temperature (since K_e and ε both increase with T_e). Overall, this analysis illustrates that one of the most notable and interesting properties of microplasmas is the potential to separately control two system temperatures (electron and gas temperature) simply by reducing the size of the plasma. Combined with the parameters previously discussed (e.g. electrode cooling, convective gas flow, gas composition, etc), this provides a set of additional control 'knobs' to tune the non-equilibrium environment. Thus, microplasmas offer a wide range of process conditions for the synthesis of nanomaterials, with the possibility of exploring new operating regimes (i.e. pressures above atmospheric) [77].

The simplified 0D analysis above provides significant insight into the effect of plasma confinement on the energy balance and local thermodynamic equilibrium, i.e. the electron and neutral gas temperature. However, plasma confinement has other more complicated implications that are not captured by this analysis. In particular, plasma confinement can lead to higher electric fields near the electrode surface and atypical charge distributions. Experimental and simulations results will be discussed in the next section which clearly show this relationship [5, 9]. Here, in order to continue with our 0D analysis, the Debye length is considered.

The Debye length is one of the traditional parameters that have been used to characterize plasmas and is given by $\lambda_D = (\varepsilon_o k T_e/(n_e q))^{1/2}$, where ε_o is the electric constant, k is the Boltzmann constant and q is the elementary charge. If a plasma is confined to a cavity comparable in size to the Debye length, shielding of the charge by the plasma and quasineutrality may no longer be preserved [54]. For plasmas with an electron temperature of 3 eV and an electron density of $10^{16}\,m^{-3}$, a typical Debye length is approximately 10^{-4} m. Since microplasmas have been found to contain larger electron densities ($\sim 10^{18}\,m^{-3}$) and slightly higher electron temperature [5, 63, 69, 78, 79], a departure from Debye shielding would probably occur at dimensions of 10^{-4}–10^{-5} m. For sustainment to occur at these conditions, a plasma cannot be governed by the same mechanisms as in the case where the Debye length is orders of magnitude smaller than the plasma volume. Therefore, a regime of plasma operation may exist where the conventional definition of Debye length is no longer applicable. When a transition to this new regime occurs, the electron density distribution is incompatible with long-range steady-state plasma neutrality, as established by the Debye length, and the plasma can be sustained and achieved only dynamically [22] (this will be briefly discussed in the next section). Overall, the instantaneous charge imbalance can be used to define the MPR and, consequently, the classical definition of a plasma is challenged [51, 54].

2.2. *Simulation and experimental investigations of the MPR*

As previously described, the properties of a plasma, including its structure, electron density and charge neutrality, can be significantly perturbed by progressively reducing the electrode gap. One of the possible sources of perturbation is the large electric field that exists before ignition and remains after breakdown within a plasma formed at small gaps (i.e. $<100\,\mu$m).

For dc microplasmas, the effect of increasing the surface-to-volume ratio is readily observed and, consequently, non-equilibrium plasmas at atmospheric pressure have been sustained at gap distances of a few hundred micrometres [65, 66]. However, the charge neutrality [68] and discharge structure [65, 66, 82] are relatively undisturbed at these dimensions. In order to observe deviations due to electrode spacing such as charge re-distribution, dimensions below $100\,\mu$m are required [80–82]. Recently, there has been a renewed interest in a fundamental understanding of ignition mechanisms at these small electrode gaps. Deviations to the Paschen law have been observed for dc microplasmas by many research groups and linked to the existence of large electric fields near the cathode surface [80, 81, 83–86]. In some cases, this has been related to secondary electron emission and in others, to electron field emission. Generally, the presence of large electric fields will create electrons with high energies and, therefore, produce an EEDF with a pronounced high-energy tail [51]; this has been verified by experiments and simulations of low- and high-pressure microplasmas [5, 69, 70]. At low excitation frequencies (<1 MHz), the characteristics of the plasma are found to be close to dc behaviour as the mean free path is at least an order of magnitude lower than the electrode spacing. Although dc and low frequency power are simpler to use, increasing the frequency of excitation leads to other advantages including a modification of the charge balance [87].

Two interesting simulations have been performed by Iza *et al* and Shi *et al* on microplasmas operated at 13.56 MHz with parallel-plate electrode configurations to elucidate their physical structure [5, 88]. Calculations showed the presence of high-energy electrons with energies as high as 21 eV and suggested that charge neutrality was only preserved dynamically in a small region that oscillates between the electrodes. Figure 3 shows the spatiotemporal profile of the electron density obtained by Shi *et al* as a function of the electrode gap [88]. As the gap decreases from 0.8 to 0.3 mm, a clear transition is observed from a traditional

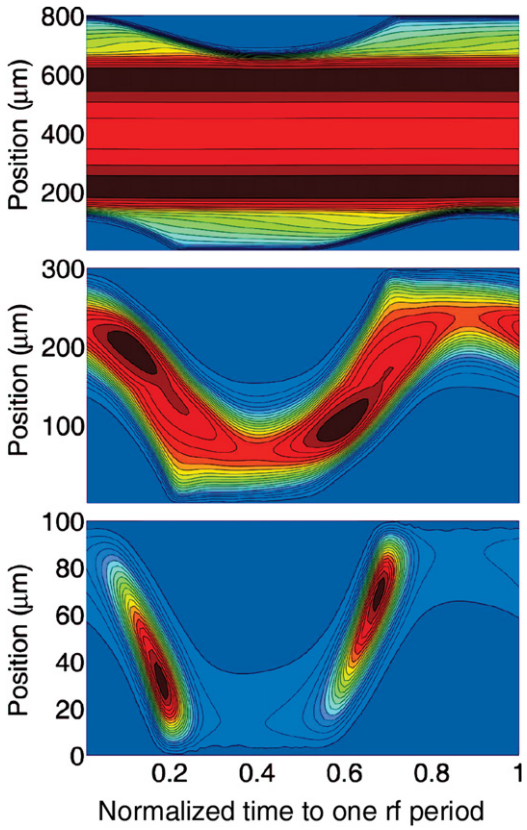

Figure 3. Spatiotemporal profile of the normalized electron density for rf atmospheric-pressure microplasma in He with an electrode gap of (top) 0.8 mm, (middle) 0.3 mm and (bottom) 0.1 mm. Reprinted with permission from [88], copyright 2006 American Physical Society.

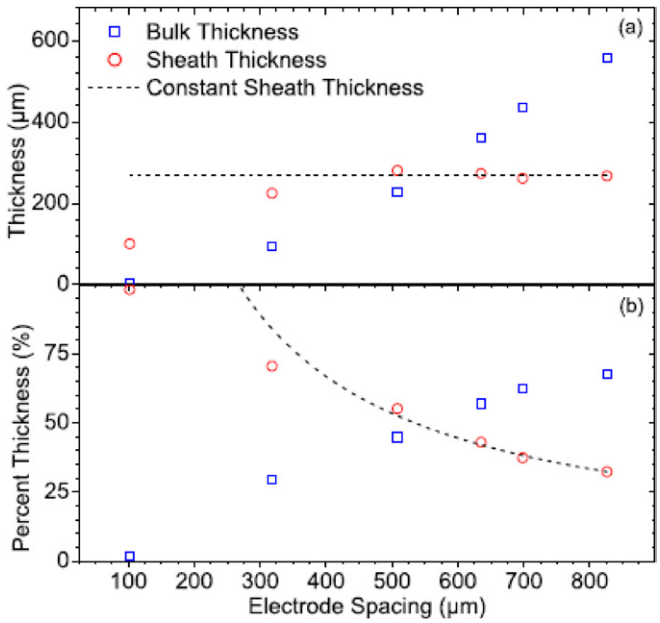

Figure 4. Calculated sheath and bulk thicknesses (from electrical measurements), for atmospheric-pressure He plasma operated at 13.56 MHz in a parallel-plate configuration, as a function of (*a*) gap size and (*b*) per cent of the electrode spacing. The dotted line represents constant sheath thickness. Reprinted with permission from [9], copyright 2009 American Physical Society.

sheath–bulk–sheath structure at larger gaps to a region of high electron density that oscillates between the electrodes at smaller gaps. The characteristic length scale where this transition occurs (∼0.3 mm) may represent the MPR with unique and favourable conditions for nanomaterials synthesis. For instance, appropriate control of the high-energy electrons may open specific chemical reaction pathways. At even smaller gaps of 0.1 mm, this concentration of high-energy electrons appears and disappears every half rf cycle with subsequent electron losses. Since the simulation did not consider the effect of heating, we suspect this regime would eventually lead to thermal instabilities.

Simulations of plasmas formed in small gaps have been supported experimentally by several reports [9, 72]. Electrical measurements were used to determine the structure of the microplasma, and showed that the sheath shrinks with reduced electrode gaps [9]. Figure 4 shows that the sheath thickness is, as expected, independent of the electrode gap until about 0.4 mm when there is a sudden decrease with further reduction in gap spacing. This transition occurs at the same electrode spacing where the oscillating electron density was observed (middle of figure 3) and may be a result of plasma confinement. Additional effects due to an increasing surface-to-volume ratio are shown by the relationship between power density and thermal equilibrium. The qualitative analysis previously discussed and shown in figure 2 has been validated by experiments [9]. In figure 5, curves that separate non-equilibrium from thermal equilibrium are shown for different values of power density; as predicted, the thermal equilibrium curve shifts down and to the right with increasing power density. The calculations indicate that in order to sustain a non-equilibrium plasma at atmospheric pressure *and* higher power densities, it is necessary to reduce the electrode gap. For example, an atmospheric-pressure plasma sustained at a power density of 145 W m^{-3} within a 100 μm electrode gap exhibits a gas temperature close to room temperature (see figure 5) while a plasma jet with a 7 cm diameter at the same power density has been found to be close to thermodynamic equilibrium [89]. This analysis highlights another important property of microplasmas: the ability to achieve a non-equilibrium plasma at very high power densities which was previously thought to be difficult.

Optical emission spectroscopy (OES) has been used to detect and confirm the presence of high-energy electrons that are not in local equilibrium with the electric field [72]. Given the strong spatiotemporal variations that exist in a plasma formed over small dimensions, precise measurements require a spatial resolution of at least ∼0.01 mm at a rate at least 10 times faster than the excitation frequency. Attempts to perform probe-based measurements have been reported [90], although the size of the probe (∼0.3 mm in diameter) is still too large for meaningful diagnostics. For this reason, OES remains the most powerful diagnostic method for microplasmas and has been widely used to analyse a variety of properties ranging from gas and electron temperature to quantification of the densities of various chemical species [91–93]. Spatial resolution has been achieved better than 0.01 mm by OES [94] and with a chromatic-free microscope

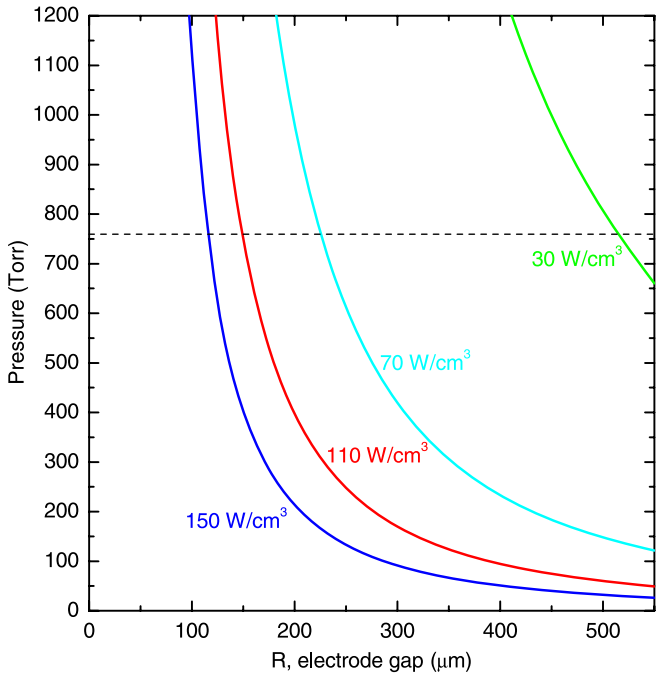

Figure 5. Thermal equilibrium curves at different power densities calculated from experimental conditions [9]. The dashed black line indicates atmospheric pressure.

mirror system [95]. Very fast acquisition times have allowed optical characterization of a 6.78 MHz microplasma with sufficient spatial resolution to produce space-time emission maps of 0.3 mm gap discharges [72].

OES has also been used in conjunction with collisional–radiative models to determine traditional plasma parameters such as electron density and electron temperature [96, 97]. Effective electron temperatures have been measured as high as 14 eV [63]. An alternative approach based on Thomson scattering has reported electron temperatures of about 1 eV [98]. While Thomson scattering is a promising and accurate technique, spatial resolution remains a challenge. This technique has also been used to determine the electron density, with values as high as 10^{20} m^{-3} [98]. Alternatively, millimetre wave transmission [99] and broadening of the hydrogen emission line have been used to measure electron densities and estimated to be between 10^{19} m^{-3} and 10^{21} m^{-3} [9, 100–105]. Experimental techniques for measuring the gas temperature are well established and straightforward due to the relatively small space-time variations associated with the neutrals. In addition to thermocouple measurements [106] and thermal imaging [101], optical monitoring of molecular emission bands for OH and N_2 has revealed that a range of temperatures exist from room temperature up to 2500 K [100, 102–105].

To summarize, experiments and simulations of plasmas at reduced electrode gaps (less than ~0.5 mm) and high frequencies (~1–20 MHz) have shown the following characteristic features [9, 72, 88]: (1) the sheath thickness scales with the electrode gap, (2) the plasma is almost fully capacitive, (3) non-equilibrium conditions exist at high power densities (>30 W cm^{-3}), (4) the bulk plasma contains a population of energetic electrons that oscillate between the electrodes and (5) these electrons are not in local equilibrium with the large electric fields (comparable to the sheath electric field). Overall, these observations suggest that the MPR is distinct from other regimes. Although there have been far fewer studies of microplasmas operated at higher frequencies (>20 MHz), it is apparent that with increasing frequency of power, changes in the charge distribution and a transition to the MPR might occur at larger electrode gaps. We speculate that at higher frequencies, the charge has less time to build up on the electrode surface, resulting in smaller electric fields near the electrode and, subsequently, lower concentrations of high-energy electrons. Experimental measurements of microplasmas operated at 450 MHz confirm non-equilibrium characteristics, probably due to volume confinement, up to 0.7 mm [63, 78]; however, there are no reports as of yet with more detailed information on a MPR beyond 13.56 MHz.

Modelling has provided a wide range of information about microplasmas including electron and ion densities and the EEDF. While simulations have helped establish some of these parameters, gas temperature effects have not been included. It is now clear that for a complete understanding of microplasmas, as well as for applications such as nanomaterials synthesis, heating effects cannot be ignored [107]. Looking forward, further progress is required to comprehensively characterize the plasma parameter space, and, in particular, obtain details of the EEDF. If the effective electron temperature is not sufficient to guide microplasma-based processes, space- and time-resolved measurements of the EEDF will be necessary to confirm the results of simulations and advance microplasma science and technology. In addition, diagnostic techniques must continue to improve to support and guide modelling efforts. Although sophisticated and/or self-contained collisional–radiative models are a potential solution, new approaches to diagnostics will also be needed.

3. Synthesis of nanomaterials

Over the last decade, there has been a rapid rise in the number of reports in the literature that discuss applications of microplasmas for nanomaterials synthesis. The broad range of configurations that have been explored illustrates the versatility of microplasma sources, but also makes a comprehensive classification of all the studies quite daunting. Nonetheless, there are some common features; for example, most of the configurations that have been used for nanomaterials synthesis are continuous and operated at steady state. As stated earlier, this is not surprising since continuous processes are particularly useful for nanomaterials synthesis to control the nucleation and growth, and ease collection of product. Many of the experiments involve a single microplasma source to prepare materials locally, sufficient for lab-scale studies, but a potential drawback for large-scale applications. Otherwise, the experimental details of each process vary quite dramatically and can be differentiated by various process parameters such as the electrode geometry, frequency of the power coupling, specific material chemistry, method of introducing precursor and how the product is collected.

Table 1. Classification of microplasma systems and configurations that have been used for nanomaterials synthesis (Cap. = capacitive coupling; Ind. = inductive coupling; NP = nanoparticles; NS = nanostructures; NT = nanotubes; NSF = nanostructured films; NC = nanocrystals).

	AMP configuration	Power coupling	Structures	References
(a)	Hollow-cathode metal tubes	Cap. dc/15–35 kHz Tube–Tube/Single	Si-NCs Ni-NPs Fe-NPs Ni_xFe_{1-x}-NPs C-NTs	[111, 113, 116, 119, 182]
(b)	Gas jets with external electrodes	Ind./Cap. 144 MHz Coil–Coil/Ring–Ring	Si-NPs Si-NCs	[117, 118]
(c)	Gas jets with wire electrode *(wire is used as metal precursor in some cases)*	Ind./Cap. 450 MHz (Pulsed) Coil/Patch-Wire	Au-NPs C-NSs C-NTs Mo-NSFs MoO_x-NSFs MoO_x-NSs WO_x−NSs	[47, 60, 124–134]
(d)	Gas jets with tube electrode	Cap. 13.56/14 MHz Single Tube/Tube-wire	Si-NSs C-NSs C-NTs	[120, 138–140]
(e)	*In situ* deposition for inner microcapillaries	Cap. 13.56 MHz/50 kHz Plate/Ring-Plate	TiO_x-NSs C-NTs	[121–123]
(f)	Plasma–liquid interactions	Cap. DC/13.56 MHz Tube-liquid	Ag-NPs Au-NPs C-NS TiO_2-NSF	[159–162, 164–168]

Here, we have chosen to focus on studies aimed at producing truly nanoscale materials (less than 100 nm in at least in one dimension and in most cases less than 10 nm) and categorized the reports by the phase of the precursor that was used, i.e. gas, solid or liquid, which appears to be an important issue for describing the growth mechanism in the microplasma. For example, some schemes have followed standard practices that have been used for low-pressure plasma processing, introducing molecular gases (i.e. CH_4, SiH_4), saturated vapour streams of solid or liquid precursors (i.e. ferrocene, tetraisopropoxide) or atomized/nebulized flows of liquid precursors, into the microplasma volume to nucleate nanoparticles or other nanomaterials from gas-phase radicals. Alternatively, to grow nanomaterials from a solid, a very different mechanism has been exploited where metal wires are used as an electrode and evaporated in a microplasma by a controlled process, given that sputtering is reduced at higher pressures. A more recent direction is the coupling of microplasmas to liquids to grow materials in solution by initiating electrochemical reactions such as anodic dissolution of solid electrodes or electroreduction of dispersed metal salts. In table 1, we have provided a brief summary of some of the different techniques that have been reported. Below, these and other reports are described in more detail.

3.1. Gas-phase nucleation from vapour precursors

Gas-phase nucleation of nanomaterials in a microplasma from vapour precursors is a natural extension of previous studies with low-pressure plasmas [39] and larger-scale atmospheric plasma jets [108]. There are many different precursors that are available, generally referred to as chemical vapour deposition (CVD) or metal-organic chemical vapour deposition (MOCVD) precursors, that can be non-thermally dissociated in a microplasma to grow different types of materials (i.e. metals, semiconductors and oxides). The general mechanism for nucleation, schematically shown in figure 7 for the case of SiH_4 vapour, is to introduce the precursor in the microplasma and form reactive radical species, such as SiH_3, by electron impact dissociation. These radicals can collide, react and nucleate small clusters at the appropriate process conditions. The clusters will then grow, by additional radical or vapour deposition on the particle surface, or agglomerate, through collisions with other particles. Finally, the particles will exit the microplasma volume as an aerosol flow.

The very first demonstration of gas-phase nucleation in a microplasma was carbon nanomaterials by Shimizu *et al* [109]. In that work, the source configuration consisted of a quartz capillary tube with a tungsten wire inserted inside as an electrode. A second electrode was placed as a coil on the outside of the capillary tube and the microplasma jet was operated with ultra high-frequency (UHF) power. Experiments were performed with gas mixtures of CH_4 (0.5%) and Ar flowing through the microplasma into air and products deposited directly onto metal substrates. Different powers were found to induce morphological changes in the deposited film with the most promising result being the observation

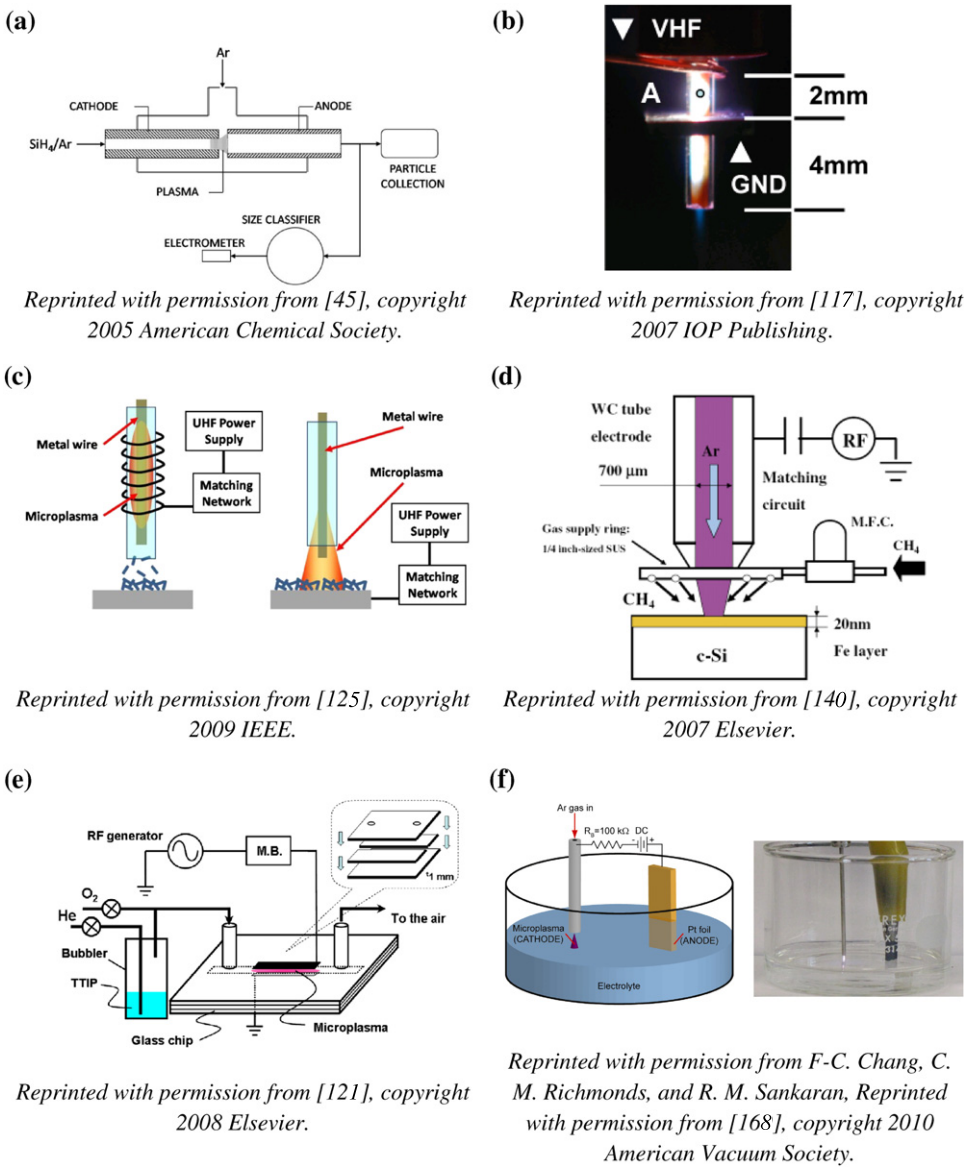

Reprinted with permission from [45], copyright 2005 American Chemical Society.

Reprinted with permission from [117], copyright 2007 IOP Publishing.

Reprinted with permission from [125], copyright 2009 IEEE.

Reprinted with permission from [140], copyright 2007 Elsevier.

Reprinted with permission from [121], copyright 2008 Elsevier.

Reprinted with permission from F-C. Chang, C. M. Richmonds, and R. M. Sankaran, Reprinted with permission from [168], copyright 2010 American Vacuum Society.

Figure 6. Typical microplasma configurations used for nanomaterial synthesis; each figure corresponds to the description provided in table 1 and in the text.

of spherical nano-onions about 30 nm in diameter. Carbon nanomaterials such as nanorods have also been synthesized in pulsed microplasmas formed in pure CH_4 [110].

Later studies have used a different electrode geometry and power coupling to nucleate and grow nanomaterials from vapour precursors. Sankaran *et al* used a stainless-steel capillary tube and mesh as the cathode and anode, respectively, to form a dc microjet and synthesize Si [45], Fe [111] and Ni [111] nanoparticles (figure 6(*a*)). The particles were generated in the gas phase and detected by an aerosol size classification system which was directly coupled to the continuous-flow, atmospheric-pressure microplasma as an on-line diagnostic tool [112]. The *in situ* measurements of the as-grown particles, along with careful control of the precursor vapour concentration, were essential to optimizing reactor conditions for the preparation of narrow distributions of ultrasmall nanoparticles less than 5 nm in diameter [113]. Figure 8 shows steady-state aerosol results for Ni nanoparticles synthesized in a microplasma from sublimed vapours of nickelocene in Ar. At 2.0 ppm, the geometric mean diameter and standard deviation, obtained by a log-normal fit, were found to be 2.2 nm and 1.13, respectively. Compared with low-pressure plasma experiments [114], the particles synthesized by this route are much smaller because of the shorter residence times [45]. Additionally, atmospheric-pressure operation reduces the minimum concentration of precursor required to nucleate particles and minimizes safety-related issues related to handling of dangerous gases or other chemicals [115]. As the precursor concentration was raised to 2.6 ppm and 5.2 ppm, the mean diameters shifted to 3.1 nm and 4.7 nm, respectively, while the standard deviations increased slightly to 1.16 and 1.22, respectively. This observation is explained by the general mechanism in figure 7; at higher precursor concentrations, the density of radical species should increase in the microplasma, driving particle growth and leading to larger mean diameters. Aerosol measurements were confirmed

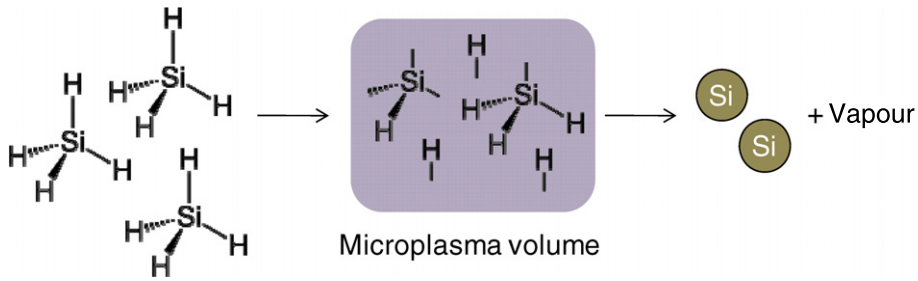

Figure 7. Hypothesized mechanism for gas-phase nucleation of Si nanoparticles from silane vapour in a continuous-flow microplasma. Radical moieties (e.g. SiH_3, H, etc) are generated in the microplasma volume by electron impact dissociation and react to nucleate Si clusters. The excess vapour contains gaseous byproducts such as H_2.

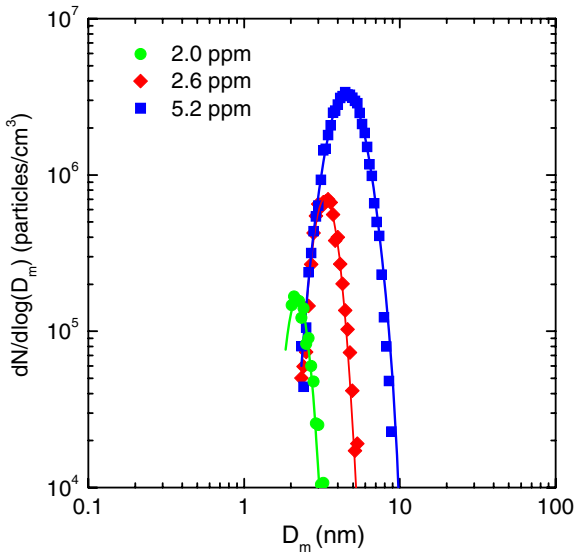

Figure 8. Aerosol measurements of as-grown Ni nanoparticles synthesized in a microplasma at indicated vapour concentrations of nickelocene in Ar. Adapted with permission from [113], copyright 2008 American Chemical Society.

by collecting the nanoparticles and performing transmission electron microscopy (TEM) analysis (figures 9(*a*)–(*c*)). High-resolution images reveal that the particles grown by this method are spherical and crystalline (see insets of figures 9(*a*)–(*c*)). The lattice spacing of 0.20 nm observed for one particle is comparable to the (1 1 1) crystalline plane of bulk Ni (figure 9(*b*) inset). Histograms obtained by sizing and counting particles in the corresponding TEM images (figures 9(*d*)–(*f*)) were found to be in good agreement with aerosol results. Overall, these studies reflect the promise of microplasma-based synthesis routes for continuous and tunable preparation of high-purity nanometre-sized (i.e. 1–5 nm) particles at atmospheric pressure.

A distinct advantage of nucleating nanoparticles in a microplasma from a vapour source is the ability to mix different precursors to synthesize bimetallic or alloyed nanoparticles [116]. This has been demonstrated by the formation of Ni_xFe_{1-x} nanoparticles from vapours of nickelocene and ferrocene, where x refers to the atomic concentration of Ni in the as-grown bimetallic nanoparticles. The ratio of Ni to Fe was tuned by varying the relative vapour concentrations of the respective metallocenes while the mean size of the bimetallic nanoparticles was controlled by the total precursor vapour concentration in Ar. We note that the actual amount of Ni and Fe in the nanoparticles was confirmed with *ex situ* materials analysis discussed below. Figure 10(*a*) shows a TEM micrograph of bimetallic nanoparticles synthesized from a relative vapour concentration of 27 : 73 nickelocene : ferrocene. The particles are spherical, crystalline and unagglomerated, similar to as-grown monometallic Fe and Ni nanoparticles. High-resolution TEM of a representative particle shows a lattice spacing of 0.21 nm, slightly larger than the (1 1 1) crystalline plane for Ni nanoparticles (figure 10(*a*) inset). The chemical composition of individual nanoparticles was assessed by energy-dispersive x-ray (EDX) spectroscopy (figure 10(*b*)). The ratio of the intensities of lines corresponding to Ni Kα and Fe Kα radiation for three samples grown with varying relative amounts of metallocene vapour confirms that the particle composition is precisely tuned by controlling reactor conditions. To evaluate the crystalline or alloy structure of the bimetallic nanoparticles, x-ray diffraction (XRD) was employed. The XRD patterns of the same three samples show that when Fe is incorporated into a Ni nanoparticle, the Ni face-centred cubic (fcc) structure expands slightly (figure 10(*c*)). At high atomic fractions of Fe (>50%), the bimetallic nanoparticles also exhibit body-centred cubic (bcc) crystal structure, as indicated by the appearance of new diffraction peaks (see figure 10(*c*)). Overall, the aerosol results combined with materials analysis demonstrate that microplasma synthesis is capable of independently tuning the size and composition of nanoparticle alloys (figure 10(*d*)).

While dc coupling is convenient for igniting and sustaining microplasmas since it precludes the need for matching networks, there are several drawbacks. As in the case of low-pressure dc glow discharges, the power consumption is higher than if high frequency (i.e. ac, rf or higher) is used, leading to power losses and thermal effects (i.e. ion heating). Perhaps more important for materials applications, the electrodes must be conductive and in contact with the reactive plasma which may result in contamination of the as-grown material. To address these issues, Nozaki *et al* developed a VHF (very high frequency = 144 MHz) powered microplasma with metal electrodes surrounding a quartz capillary tube [117, 118]. In his experiments, $SiCl_4$ was used as a vapour precursor to produce Si nanocrystals that were directly deposited downstream of the microplasma onto

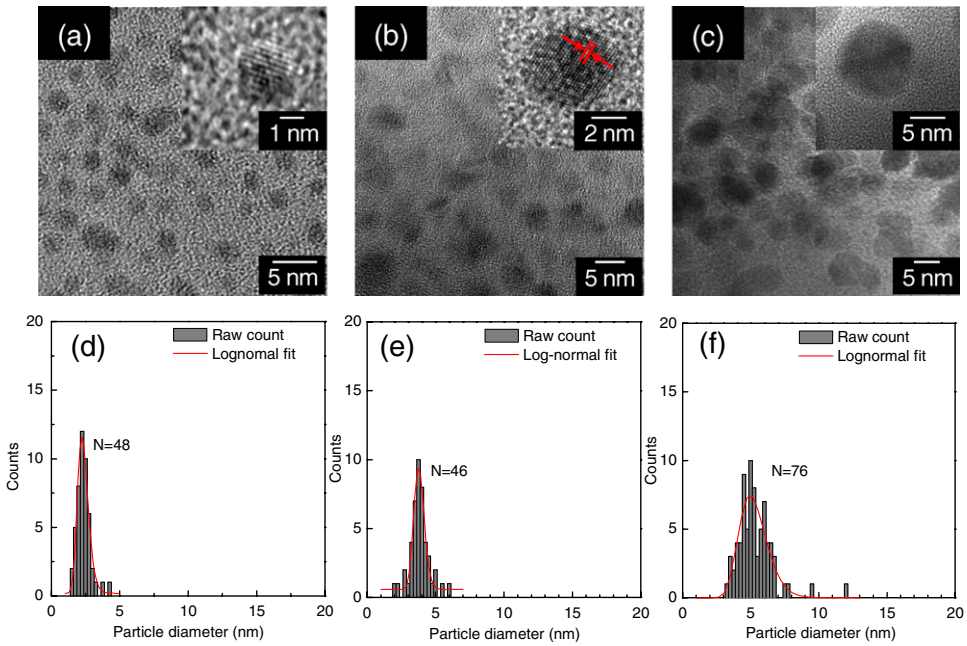

Figure 9. TEM analysis of as-grown Ni nanoparticles prepared in an atmospheric-pressure dc microplasma at various nickelocene vapour concentrations in Ar of (*a*) 2.0, (*b*) 2.6 and (*c*) 5.2 ppm (inset: HRTEM image of a Ni particle exhibiting a lattice spacing of 0.20 nm). Histograms of Ni nanoparticles obtained from corresponding TEM images for nickelocene vapour concentrations in Ar of (*d*) 2.0, (*e*) 2.6 and (*f*) 5.2 ppm. Adapted with permission from [113], copyright 2008 American Chemical Society.

glass substrates. By adjusting the H_2 concentration in the microplasma, the deposition rate and particle size were tuned to obtain size-dependent room temperature photoluminescence, a very promising result for optical applications. Rf powered atmospheric-pressure microplasmas have also been implemented for carbon nanotube (CNT) growth [119, 120]. Discharges were formed in CH_4/H_2 mixtures with a catalyst loaded on a substrate to nucleate and growth CNTs.

The small physical size of a microplasma source permits localized synthesis or modification of materials. Surface treatment of the inner walls of microscale cavities is attractive for microfluidic applications such as electrophoretic analysis of proteins and DNA, zeta potential measurements or microreactors [121–123]. These applications generally involve dielectric materials such as quartz microcapillaries making it necessary to use capacitive or inductive power coupling for plasma generation. Previous studies have used He as the carrier gas with parallel-plate electrodes placed across [121, 122] or at the ends of the capillary [123]; this has allowed for the plasma to expand up to 6 cm in length along the capillary axis (internal diameter 0.5–1 mm). The simplicity of these experimental approaches allows gas mixtures containing precursors to be injected on one side of the capillary and exit on the other side into air to produce coatings on the inner surfaces.

One of the major challenges for coating applications is the uniformity of surface coverage since the boundaries of a plasma may be characterized by gradients in the radical composition [121]. In addition, the precursor composition itself could vary along the direction of the gas flow in the microcapillary as it is consumed during deposition. Improvements in the uniformity of the coating may be achieved by reducing the volume of the plasma even further and translating the microplasma along the capillary axis.

3.2. Evaporation/sputtering of solid metal electrodes

A popular configuration for generation of nanomaterials in a microplasma, perhaps because it was the first to demonstrate the concept [124], is to evaporate or sputter a sacrificial metal electrode. In general, a fine metallic wire (0.03–0.3 mm diameter) is inserted inside a quartz or alumina microcapillary (0.1–0.8 mm internal diameter). The second electrode required for discharge formation is usually placed outside the capillary (see left-hand side of figure 6(*c*)), although a wide range of other geometries have also been explored [125]. The external electrode is normally coiled to facilitate its placement around small and fragile capillaries and to allow for an optical path for visual observation and optical emission measurements [126–133]. In a few cases, a patch antenna-type electrode has been placed underneath the substrate where the nanostructured material was deposited (see right-hand side of figure 6(*c*) [47, 60, 134]). This arrangement allows the plasma to interact directly with the substrate during particle formation and deposition. The power coupling is largely capacitive and only a small, likely non-influential, inductive contribution occurs. Some added benefits of inserting a metal wire into a microplasma are a lowering of the breakdown voltage and operating power. This has been explained by thermionic emission of electrons, particularly for refractory metals [137], and electric field enhancement as a result of the electrode geometry. Previous reports have almost exclusively focused on UHF operation at 450 MHz, although lower frequencies are equally capable of sustaining such microplasmas. Possible advantages for UHF excitation are lower power consumption and the ability to sustain microplasmas at low temperature and low gas flows which approach static conditions. Pulsed power at 450 MHz has been also demonstrated for the synthesis of gold nanoparticles [131].

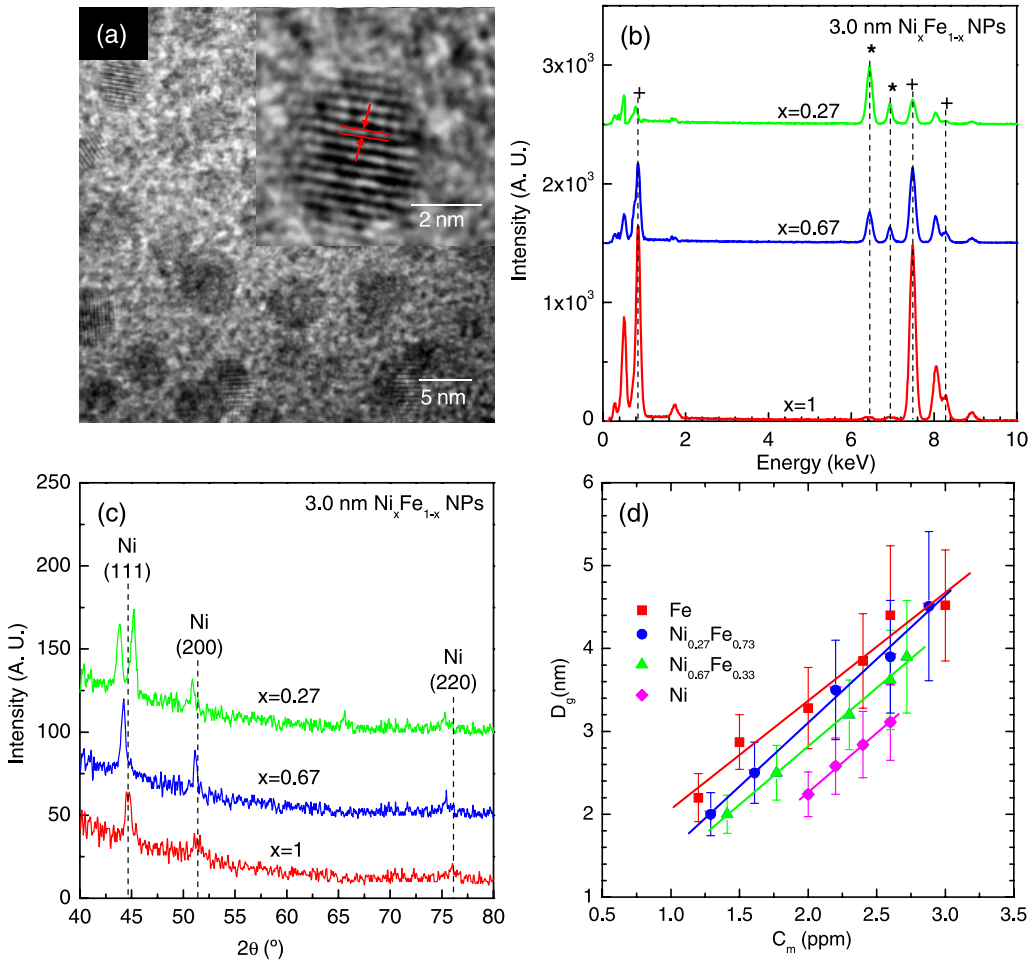

Figure 10. (*a*) TEM image of as-grown $Ni_{0.27}Fe_{0.73}$ nanoparticles prepared in a dc, atmospheric-pressure microplasma at a vapour concentration of 1.97 ppm ferrocene + 0.50 ppm nickelocene in Ar (inset: HRTEM image of a particle exhibiting a lattice spacing of 0.21 nm). (*b*) EDX spectra of Ni_xFe_{1-x} (x = Ni at%) nanoparticles with Ni (+) and Fe (*) peaks indicated. (*c*) XRD characterization of Ni_xFe_{1-x} (x = Ni at%) nanoparticles with indices for Ni fcc peaks indicated. (*d*) Geometric mean diameter of as-grown Ni_xFe_{1-x} nanoparticles versus required metallocene vapour concentration (in Ar) in dc, atmospheric-pressure microplasma. Errors bars correspond to the geometric standard deviation of the particle size distributions. The data were obtained from on-line aerosol measurements.

Several metal-oxide (Cu [130], W [130], Mo [60, 125, 128, 134], Fe [130], Zn [105]) and pure metal (Au [131], Mo [126, 132]) nanostructures have been prepared from the respective metal wire precursors. A drawback of also using the wire as an electrode is that there is limited control over the wire position with respect to the capillary walls and, therefore, with respect to the external electrode. Variations in the radial or axial distance of the wire from the external electrode may affect the kinetics of the surface reactions and possibly the morphology/phase of the as-grown nanostructures [60]. Nonetheless, highly reproducible results have been obtained for deposited nanostructured coatings and various nanoparticles and nanostructures [60, 134]. Another potential limitation is the consumption of the wire electrode over time. Complete deterioration of the wire can occur within minutes and cause the process to be shut down; continuous operation for longer times will require some solution such as a wire-feeding apparatus.

The temperature at the wire surface and of the gas (i.e. neutrals) can be controlled by varying the gas flow rate, input power and the electrode geometry. Heating of the wire is generally attributed to inductive coupling [130], but other forms of heating may also contribute including ohmic and heat evolved from exothermic reactions (e.g. oxidation). Gas temperatures have been determined by spectroscopic techniques and found to be in the range 700–1800 K [63, 78, 105]; however, the lower bound was limited by the low intensity of the emission and it may be possible to operate at still lower temperatures, down to room temperatures. In the case of a remote microplasma, temperature-sensitive substrates have been used even at high gas temperatures (e.g. epoxy glass [130] or paper [131]). In all cases, the microplasmas are characterized by high effective electron temperatures (>2 eV) and non-equilibrium [63, 78].

Tungsten- and Mo-oxide nanostructures have been formed with average particle diameters of 20 to more than 100 nm [128, 133]. In both cases, the gas flow rate determined the size and crystalline phase of the metal-oxide nanoparticles. Higher gas flow rates were found to yield smaller particles. The crystalline phase was found to approximately vary from lower to higher oxidation state with increasing gas flow rate. EDX and x-ray photoelectron spectroscopy (XPS) characterization

of the wire after operation showed that oxidation occurred at the metal wire surface. Overall, these results suggest that at lower gas flow rates, the gas temperature is higher, leading to the evaporation of a higher flux of metal-oxide moieties that then nucleate and form nanoparticles with larger mean diameter and higher oxygen content. At higher gas flow rates, molten droplets may leave the wire surface because of the lower gas temperature which prevents evaporation of the higher melting point species such as metal oxides. This analysis has been corroborated by optical emission analysis which clearly indicates the presence of atomic Mo/W in the gas phase at lower gas flow rates. It should be noted that only small changes to the gas flow rate (i.e. 5–30 sccm) are needed to dramatically change the mechanism for particle formation. Formation of ZnO films has also recently been demonstrated with high deposition rates [105]. The preparation of other metal-oxide nanostructures such as CuO or Fe_2O_3 should also be possible.

The mechanism for evaporation and/or sputtering of metal wire sources in a microplasma is not clear as there is no comparable process. Although wire flame spraying bears some similar features, microplasma-based systems are fundamentally different from these thermal processes because of the presence of energetic species (e.g. ions and electrons) [60, 125, 126]. Since physical sputtering by ion bombardment is a function of the ion energy, we expect that sputtering may be reduced at the high pressures used in microplasmas due to collisional effects. However, the high surface temperature of the metallic wire could enhance sputtering of surface atoms at lower ion energies [105]. This picture has been complicated by experimental results indicating that Ar or He alone is usually insufficient to produce material [126, 132]. In most cases, O_2, H_2 or CH_4 are needed which implies that reactive processes are important. There are a few examples of metal-oxide nanostructures produced with only Ar and no O_2 gas [60, 105, 130, 134]. The source of O_2 for oxide formation has been attributed to either the etching of the quartz capillary [130] or outside air leaking into the gas lines. Water vapour in the gas lines may also be responsible, as supported by the presence of OH radicals in the collected spectral emission [105, 128]. Despite the uncontrolled source of oxygen, nanostructures with reproducible size and composition have been synthesized. Curiously, Ar–O_2 mixtures produce similar results [125, 133]. In either case, oxidation is believed to occur at the metal wire surface, and, unlike thermal oxidation, oxygen radicals and ions should be involved in surface reactions leading to material formation [136]. More experiments are needed to reveal the separate roles of heating and other physical and chemical processes.

Metallic nanostructures have been produced from wire sources by introducing a small percentage (<4%) of H_2 in the gas mixture. For example, various shapes of Mo [126, 132] structures and spherical Au [131] nanoparticles have been synthesized and deposited at room temperature. In the case of Au, pulse modulation of the input power was used to avoid excessive gas heating by H_2 [137]. The role of H_2 has not been clearly established, but it is likely that atomic hydrogen, formed in the plasma volume, reacts and reduces the oxide on the wire surface to allow the formation of metallic nanoparticles.

Finally, solid precursors have been introduced into a microplasma by more conventional schemes, i.e. exposure of a substrate to a reactive plasma. Fe-coated Si substrates were used to produce Si nanocones, CNTs and other nanostructures in the gas phase through a combination of etching (or sputtering or evaporation) and catalytic growth processes [138–140] (figure 6(*d*)). A drawback of this approach is that the formation and structure of as-grown nanomaterials is very sensitive to the distance of the substrate from the microplasma jet.

3.3. Plasma–liquid interactions

A relatively new direction for microplasma science and technology is applications to liquid-phase systems. While plasmas have been generated inside or on the surface of liquids in studies dating back as far as 100 years ago by Gubkin [141], Hickling [142, 143], Harada [144, 145] and others [146, 147], the use of low-pressure or thermal plasmas (i.e. arcs) has limited these previous experiments to short time scales, liquids with extremely low vapour pressures (e.g. ionic liquids) or required external cooling to prevent evaporation. The development of microplasma sources characterized by non-thermal operation at or near atmospheric pressure has now made it possible to stably interface plasmas with more common liquids, including water. This has spurred a great deal of interest for applications in water treatment [148, 149], medicine [150, 151] and chemical analysis [152, 66]. Moreover, relevant to our discussion, the formation of microplasmas with liquids opens new chemical pathways to synthesize or modify nanomaterials directly in solution [154–159].

The earliest report of a plasma in contact with a liquid to synthesize nanoparticles involved a ac plasma jet formed with H_2 gas at the surface of a dilute aqueous solution of H_2PtCl_6 [160]. The presence of H_2 gas was found to be necessary to form nanoparticles, suggesting that hydrogen radicals generated in the plasma reduce the Pt salt (i.e. $PtCl_6^{2-}$) and nucleate particles. The growth of nanoparticles was monitored by UV–vis absorption and estimated to be 1.2×10^{-5} mol min^{-1} which is comparable to other reduction techniques. Nanoparticles synthesized by this approach are spherical, crystalline, uniform and extremely small with mean diameters of 2 nm. More recently, atmospheric-pressure plasma jets have been used to reduce metal salts in solution without H_2 [161, 162]. This is particularly attractive because unlike conventional colloidal growth methods [163], metal nanoparticles are produced at ambient conditions (atmospheric pressure and room temperature), without the need for chemical reducing agents (i.e. $NaBH_4$), making the approach safe and biocompatible. Nanoparticles have been grown with and without stabilizer molecules which allows the particles to be selectively functionalized [162, 164]. Various shapes of Au nanoparticles have also been achieved by varying process parameters such as the reaction time [161] and pH [164] (figure 11).

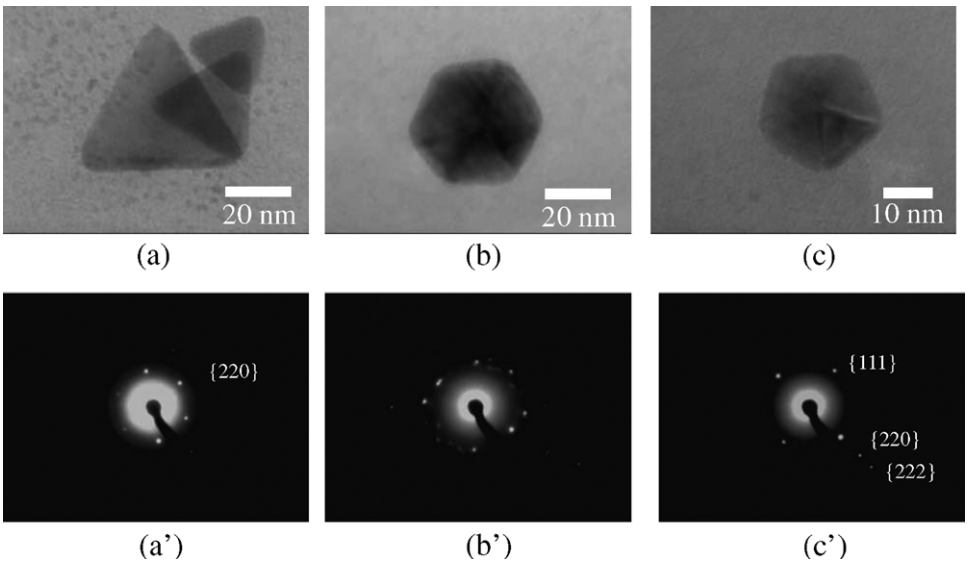

Figure 11. TEM images and corresponding electron diffraction patterns of shape-controlled Au nanoparticles synthesized by plasma discharge in aqueous solution of $HAuCl_4$. Reprinted with permission from [164], copyright 2008 American Vacuum Society.

The mechanism for plasma reduction of aqueous metal salts remains unclear, particularly when H_2 is not used in the supply gas. Plasmas formed with water could generate oxidizing or reducing agents in solution by electron impact dissociation or UV irradiation including hydrogen and hydroxyl radicals, hydrogen gas and hydrogen peroxide. When experiments are performed in air, N_2 and O_2 molecules may also be dissociated and interact with the solution [165]. Some of these highly reactive species have been proposed to be responsible for reducing the metal cations [164]. Separately, Sankaran *et al* have shown that a microplasma can initiate electrochemical reactions, similar to a standard electrochemical cell, but via interactions of gas-phase electrons with metal cations in solution [166–168]. In their experiments, a dc microplasma was formed at the surface of a solution (i.e. electrolyte) and operated as the cathode, with an immersed solid metal electrode as the anode, creating a hybrid plasma–liquid electrochemical cell (figure 6(*f*)). Igniting the microplasma resulted in current flow through the electrolyte and half cell reactions were observed at the anode and cathode. At the anode, oxidation reactions led to dissolution of the solid metal into metal cations which were then reduced at the cathode by the microplasma to nucleate metal nanoparticles (figure 12). These observations suggest that gas-phase electrons can react with a solution at the plasma–liquid boundary to drive electrochemistry. This mechanism is supported by previous reports of low pressure, large volume glow discharges formed in inert gases that have been used to directly reduce metal cations dispersed in solution [169] or on solid supports [170].

The rapidly increasing interest in the formation of plasmas in a liquid environment appears to be a natural progression of microplasma research. Moving to the liquid phase increases the density of the fluid much more significantly than increasing gas pressure and results in additional confinement of a plasma. Nanoscale plasmas have now been realized by pulsing discharges in water with a CNT electrode [66]. These highly localized, remotely generated discharges offer a potential route to grow or pattern materials directly at the nanoscale. Plasmas have also been formed at an intermediate stage in supercritical fluids [171] or cryogenically cooled gases [172]. This has allowed the synthesis of carbon nanomaterials with much higher production rates than possible in the gas phase [171]. Future studies will need to characterize the unique processing conditions afforded by supercritical fluids and liquids, but it is clear that this new regime of operation holds great promise for materials applications of microplasmas.

4. Technological applications

Despite recent progress, widespread utilization of microplasmas for nanomaterials synthesis will depend on the ability to scale up current processes to industrial level manufacturing and/or fabricate well-defined materials that are not capable of being produced by other methods. Prior research has demonstrated that there is commercial potential for microplasma-based systems in two general areas: (a) thin film deposition of nanostructured coatings, nanocomposite films and self-organized structures and (b) preparation of well-defined 'free-standing' nanostructures (e.g. nanoparticles, nanotubes) as powders or colloidal dispersions. In either case, there are several issues that must be considered including the quality of as-grown material in terms of homogeneity and structure, throughput (i.e. production rate), process cost and process safety. The quality of as-grown material depends on the desired application—for example, in some cases, the size of the nanomaterial may be important and must be precisely controlled whereas in others the composition is critical. Microplasmas are capable of producing a wide range of materials with well-defined structures and under various conditions, which could make them flexible for different applications. The throughput of material is currently a challenge since most previous studies are lab-scale and only require small amounts of material (e.g. nanograms); however, microplasmas can be operated in parallel to increase the production rate of nanomaterials.

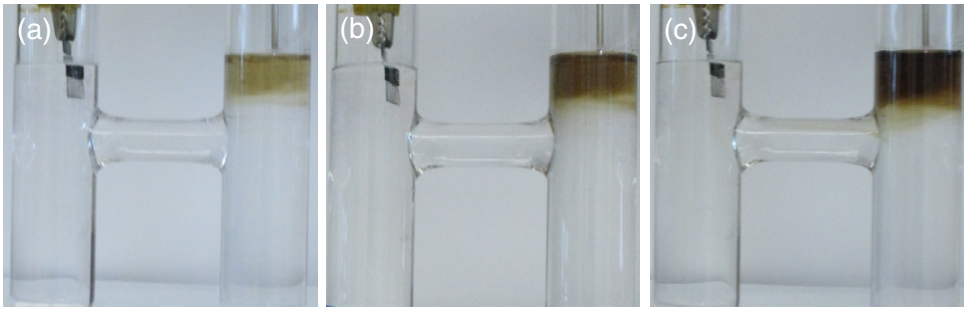

Figure 12. Microplasma synthesis of Ag nanoparticles by anodic dissolution of Ag metal and electrochemical reduction of Ag cations. Photos were taken following ignition of the discharge and operating the cell for (*a*) 5, (*b*) 7 and (*c*) 9 min. Adapted with permission from [167], copyright 2010 IOP Publishing.

Similarly, arrays of microplasma jets permit the deposition of large areas of nanostructured films and coatings. The cost of microplasma-based processes is relatively low because of atmospheric-pressure operation. In addition, one can envision the development of small-scale portable apparatuses (i.e. bench top) which may be attractive for applications with lower manufacturing requirements. In the following section, we detail some of the critical challenges that must be overcome to fully realize the potential of microplasmas for nanomaterials synthesis and applications.

4.1. Localized and nanostructured thin film applications

Material processing via microplasma jets initially attracted attention as an ideal approach for localized deposition, etching or surface functionalization of thin films. An array of microplasma jets also makes this technology competitive with other large volume, large surface area atmospheric-pressure plasmas. Microplasma jet arrays are a topic of growing interest and we will review some of the recent advances in section 4.3. First, we focus on localized materials processing by single microplasma jets. Some issues that must be considered are resolution (of the patterned film), film adhesion, coating/film uniformity, scanning speed and the ability to create self-organized nanostructures.

Previous reports have demonstrated the deposition of patterned nanostructured coatings [105, 130]. Stripes of nanostructured metal oxides have been deposited with line widths ranging from 10 μm to 80 μm [130]. The resolution of the lines was determined by the end of the quartz capillary used to form the microplasma jet ($\sim$140 μm inner diameter). This process is also compatible with temperature-sensitive substrates (i.e. glass epoxy with melting point of about 300 °C). Adhesion of deposited nanostructured films has been improved by heating the substrate while deposition occurs [105] or by subsequent annealing [130]. In the first case, adhesion was likely improved through mechanical keying which was promoted by surface roughening of the substrate (made of glass epoxy). At the perimeter of the deposited area, the surface appeared undamaged, but under the deposited material, the temperature may have been higher, allowing for improved adhesion. Insight into film adhesion and uniformity is illustrated by a recent report on thin film coatings for Li-ion batteries [134]. The as-deposited Mo-oxide nanostructured film was immersed in an electrolyte solution and successfully produced charge/discharge current measurements which showed mechanical stability and suitable adhesion to the substrate without any heat treatment. The film was deposited by scanning a single microplasma jet and analysed by SEM which revealed excellent film uniformity along the scanning direction. The film was also surprisingly uniform over a width up to at least 0.3 mm with three-dimensional (3D) architectures formed by randomly stacked MoO_3 nanosheets (figure 13(*a*)). Smaller spherical particles were observed at the perimeter of the deposit and it is likely that such particles were also forming a layer underneath the thin film (see figure 13(*b*)). A different configuration for deposition showed similar characteristics, whereby a uniform surface treatment could be achieved over a 0.4 mm diameter region; in this case, a CH_4 microplasma jet produced silicon nanocones [140]. Outside of this region, variations in the film morphology were observed, including cubic-shaped materials. Although deposition by a microplasma jet presents some challenges in terms of concentration and other gradients, careful control of the process parameters may allow further improvements in the homogeneity of as-deposited films. Future work must focus on plasma–surface interactions of microplasma jet arrays in order to deposit large areas ($\sim$1 m^2) of uniform films for applications.

The scanning speed of rastered microplasma sources is another important issue for high throughput materials processing. An upper limit for scan rate is given by e-beam processes which have speeds of 17 m s^{-1}. At this time, the highest scanning rate reported for a microplasma-based system is approximately 2 mm s^{-1} [105]. Although this value is far from e-beam technology and some other roll-to-roll deposition techniques, the current scanning speeds offered by microplasmas are still useful for applications that require atmospheric, non-equilibrium plasma processing. In the case of depositing ultra-thin nanostructured films, the scanning speed is expected to increase by at least by two orders of magnitude.

An exciting potential application of atmospheric microplasma jets is the fabrication of self-organized nanostructures. Ordering of nanostructures, as well as the formation of highly localized nanoscale wires, has been recently reported in materials deposited by microplasmas [47, 48, 125]. In one case, a CH_4 microplasma jet, similar to that depicted in

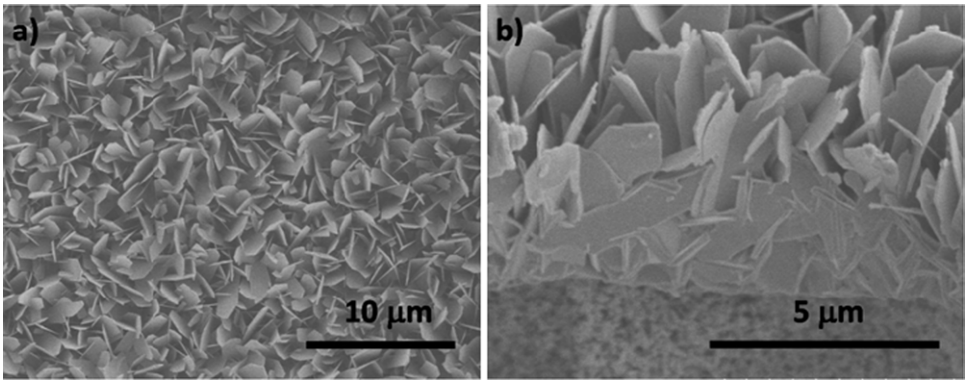

Figure 13. (*a*) Scanning electron microscope image of a nanostructured film produced by a microplasma jet; (*b*) tilted scanning electron microscope image of the same nanostructured film, which shows the thickness and underlying layer of smaller particles.

figure 6(*c*), was used to deposit carbonaceous material on a substrate with Ag nanoparticles and found to form wires between the particles [47]. Simulations in support of the experiments have revealed that during deposition, the nanostructures may charge and strong electric fields could result in preferential deposition of carbon between the nanostructures [173, 174] (figure 14). In another case, self-organization was induced by a microplasma through localized thermal gradients which caused stress and dewetting of silica films [48]. This led to the fabrication of patterned SiO_2 nanodots (∼200 nm in diameter). While these effects could occur in low-pressure plasma processes as well, the unique environment afforded by microplasmas may enhance charging and deposition, promoting the growth of self-organized architectures. Further studies will be needed to explore these interesting mechanisms for self-organization during nanostructure growth.

4.2. Preparation of 'free-standing' nanomaterials

Microplasma-based systems have been implemented and tested for continuous operation for more than 24 h with no visible deterioration, making them suitable for large-scale production [24]. One of the key questions that remain unanswered is if microplasmas can provide the required throughput of nanomaterials for industrial applications. A single dc microplasma reactor of the type shown in figure 6(*a*) has been found to produce nanoparticles at a rate of about 10^{-10} g min^{-1}. This relatively low throughput can be easily increased by arranging microplasmas as a two-dimensional (2D) array. For example, an array consisting of 10 000 microplasmas (100 × 100) would still have a relatively small foot print no larger than 1 m^2, require only a power of approximately 100 kW and achieve a production rate of 10^{-6} g min^{-1}. A drawback of this approach is that dc power is characterized by a high rate of charge losses. However, dc microplasmas are extremely simple to operate and power supplies are commercially available at low cost. If the number of microplasmas in the array can be limited to less than ∼200, other manufacturing needs could be met as well. For instance, a dc microplasma array would be suitable for niche applications such as nanoparticles for medical applications (e.g. drug delivery) where the quality of the product is more important than throughput.

As mentioned in section 2, the charge distribution and Debye length are relatively unaffected by electrode confinement in dc microplasmas. On the other hand, for microplasmas sustained with excitation frequencies above 1 MHz, the charge distribution will be significantly altered which provides an opportunity to tune the electron density and modify reaction rates. Thus, it may be possible to improve the material throughput in rf driven microplasmas, as compared with dc microplasmas. This improvement is at the expense of somewhat more complex electronics (i.e. power supply, matching network, etc) and a more carefully designed electrode configuration. Comparing microplasma systems that have been used to synthesize Si nanocrystals, it is apparent that dc power can produce high quality nanocrystals with diameters below 2 nm and a standard deviation as low as 23%, but low production rates [45]. On the other hand, a VHF-powered microplasma has shown the potential for much higher manufacturing rates, with deposition rates reaching above 4 μm min^{-1} [117]. With a few assumptions, the material throughput of a single 144 MHz powered microplasma jet can be estimated to be approximately 10^{-6} g min^{-1} which is four orders of magnitude higher than the dc microplasma. Again using the example of a 2D array of 10 000 microplasmas, the production rate is now 10^{-2} g min^{-1}. The power required to run such a system would be above 100 kW which is higher than that of a dc power system. In addition, the availability of rf power supplies with this power rating is more difficult and, therefore, arrays of only about 300–400 microplasma reactors might be feasible with commercially available systems, yielding production rates of $\sim 10^{-4}$ g min^{-1}. Overall, this value compares favourably with other techniques: 10^{-5} g min^{-1} by low-pressure plasmas [175, 176], 10^{-4} g min^{-1} by low-pressure, continuous-flow plasmas [114], 10^{-7} g min^{-1} by electrochemical etching [177, 178] and 10^{-7} g min^{-1} by laser processing in liquid [179, 180]. Further improvements in production rates will require additional knowledge of microplasma processes.

Two alternative approaches to achieving high production rates are to use solid precursors in the form of a metal wire [128, 131, 133] or liquid precursors in the form of a metal salt solution [166]. A microplasma-based system operated at 450 MHz has been used to produce Mo- and

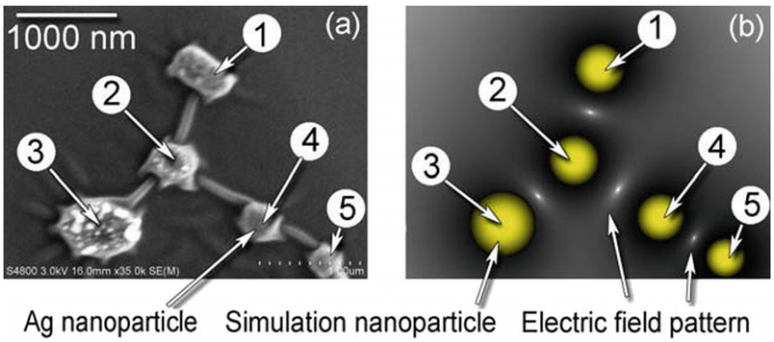

Figure 14. (*a*) SEM image of self-organized carbon nanoscale connections between silver particles; (*b*) simulated pattern with the computed 2D profiles of the microscopic electric field between the nanoparticles. Darker colour corresponds to the intensity of the electric fields showing that the strongest field gradients are localized between nanoparticles. Reprinted with permission from [173], copyright 2009 Elsevier.

W-oxide nanoparticles as a nanostructured thin film at a rate of 350 μm s^{-1} that is three orders of magnitude higher than the rate for Si nanocrystals by a VHF-powered microplasma [133]. A similar set-up was also used for the synthesis of Au nanoparticles with average diameters between 4 nm and 8 nm [131]. In solution, Ag and Au nanoparticles have been grown by reducing metal salts with a single dc microplasma jet at a rate of approximately 10^{-4} g min^{-1} [166]. This is significantly higher that the rates reported for other microplasma-based processes and holds great promise for large-scale production.

If microplasmas are not used for large-scale manufacturing, they may still find applications on a smaller scale for fundamental research. Well-defined nanomaterials are essential to basic studies in catalysis, nanoelectronics, nanomedicine or energy. An example is illustrated by a recent report that elucidated the role of a catalyst in CNT growth [113]. Precisely controlled bimetallic nanoparticles were prepared in a microplasma and used to establish a link between catalyst composition and the chirality of as-grown single-walled CNTs. This result gives insight into the mechanism for nanotube nucleation and may impact future nanotube-based electronic devices where high fractions of semiconducting or metallic nanotubes are needed [182]. More of these types of studies are expected in the near future as researchers continue to fabricate novel nanomaterials via microplasma synthesis.

4.3. Microplasma arrays

As previously mentioned, arrays of microplasmas would allow materials throughput to be drastically increased and enable large area deposition or modification of thin films. Microplasma arrays have been recently developed for applications in photonics [52], metamaterials [183], stealth technology/radar cloaking [184], medicine [185–187], environment [188, 189] and lighting or display [190–193]. In the latter case, the technology is near the commercialization stage (http://www.edenpark.com). Plasma display technology has provided motivation for the development of microplasma arrays that do not require continuous gas flow (e.g. metamaterial, photonics etc). The synthesis of nanomaterials will require the integration of gas flow, including reactive gases, creating new challenges for the design and fabrication of suitable microplasma arrays. Fortunately, many of these issues are common to other applications such as thin film deposition and medical applications and are already being addressed [186].

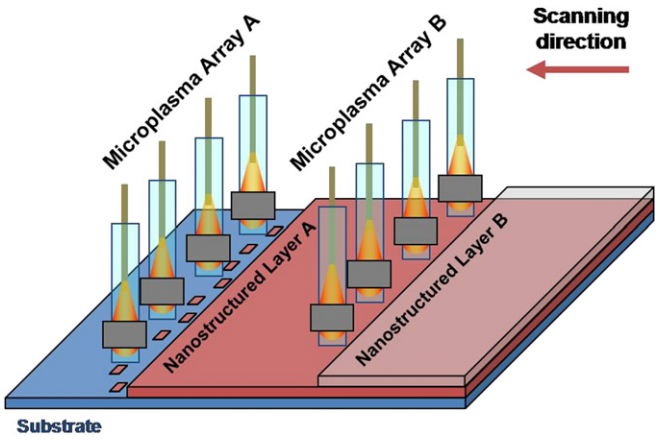

Figure 15. A combinatorial approach based on arrays of microplasma jets for low cost, roll-to-roll, large area deposition of nanostructured coatings.

In materials processing, single atmospheric-pressure plasma jets have been explored for many years and larger-scale plasma jets are now commercially available for surface treatment. The first attempts to use microplasma arrays for material processing were inspired by display applications and generated without gas flow in hollow-cathode or co-planar electrode configurations for etching and deposition [12, 23, 38, 56, 83]. Later, an array of four microplasma jets was used to deposit microcrystalline diamond films [24, 25]. While there are no reports to our knowledge of microplasma arrays for nanomaterials synthesis, there is sufficient need for large area deposition of nanostructured coatings and aerosol synthesis, as previously described. Moreover, microplasmas arrays operated with varying conditions in individual elements could lead to combinatorial approaches to materials synthesis that allow rapid optimization of process parameters to synthesize desired materials (see figure 15).

To date, the most significant progress towards fabrication of large microplasma arrays with gas flow has been achieved by

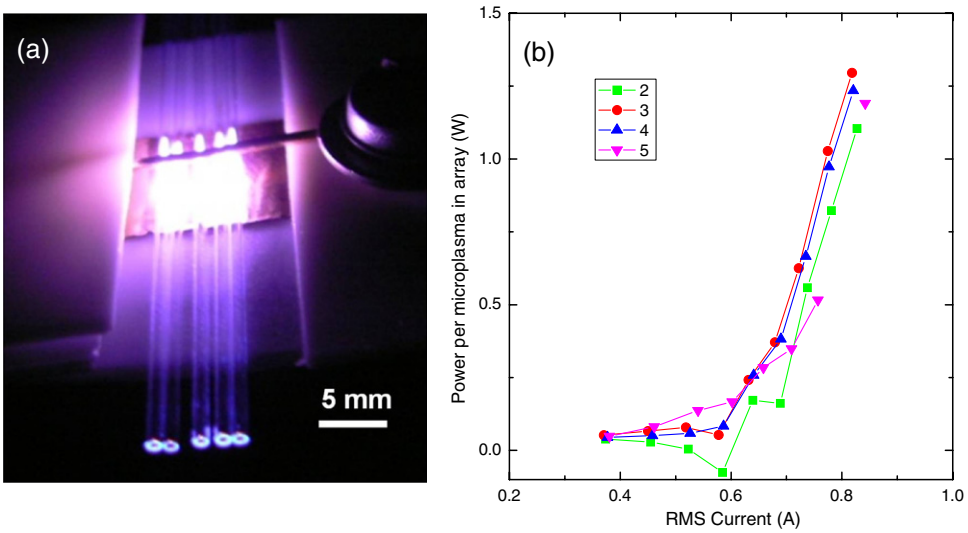

Figure 16. (*a*) An array of five microplasma jets formed in He sustained by 13.56 MHz power. (*b*) Power consumed as a function of number of microplasmas sustained in the array. The numbers in the legend specify the number of microplasmas.

researchers interested in medical applications [185, 186, 194]. Arrays consisting of seven to ten microplasma jets have been carefully characterized and a 37-jet has been fabricated. Microplasmas were generated inside quartz capillaries arranged as a square lattice either linearly or in a honeycomb geometry. The excitation frequency was varied between 5 and 30 kHz and, interestingly, lower frequencies were found to produce more uniform discharge behaviour. The instabilities at higher frequencies were most likely caused by capacitance effects since the experiments relied on cross-capacitance between the individual jets to ballast the microplasmas. Preliminary studies also showed that the arrays provided more uniform coverage for surface modification than a single jet, an encouraging result for potential thin film applications of microplasma arrays.

Although the requirements for nanomaterials synthesis are somewhat different than medical applications, these prior reports are useful as they provide insights into the technological challenges that must be overcome to scale up microplasma arrays. For example, cross-interaction between individual microplasma jets must be curtailed to achieve film uniformity. In the case of dc-powered arrays, the discharge current has been found to increase with the number of tubes while the discharge voltage remains constant, demonstrating that for smaller arrays (<10), scale-up is relatively straightforward [24]. However, to operate larger arrays with dc power, individual ballast resistors must be used to form uniform discharges and any small instabilities could cause significant problems. In addition, microplasma arrays sustained with dc power require a two-electrode configuration which drastically limits system flexibility and limits the length of the jet. In terms of power coupling, rf or higher frequencies have some advantages over dc or frequencies in the kilohertz range [185]. For large arrays (>10), rf frequencies or higher can achieve excellent stability with a single power system. Some initial work has been carried out to evaluate the electrical characteristics of an array of five microplasma jets. The set-up shown in figure 16(*a*) consisted of five quartz capillaries (1 mm external diameter; 0.7 mm internal diameter) operated in parallel. Helium was used as the supply gas and the array were sustained with rf power at 13.56 MHz. Similar to dc-driven microplasma arrays, the discharge voltage was found to be independent of the number of microplasmas in the arrays. In contrast, the current was also unaffected by the number of microplasmas. As the number of ignited jets was increased from 1 to 5, only the power was observed to increase linearly (figure 16(*b*)). Increasing the number of microplasmas apparently only affected the phase angle between the discharge voltage and current. Since each microplasma in the array introduced a resistive component without significantly altering the overall impedance of the array, the latter was largely determined by the overall system capacitance. This result is potentially useful for operation of large arrays of microplasmas which can be treated as a large-scale plasma with an equivalent effective capacitance.

5. Conclusions

In this review, we have summarized recent progress on applications of microplasmas for nanomaterials synthesis. The physical properties of microplasmas offer unique capabilities, as compared with large volume, low-pressure plasmas, for the synthesis of a wide range of nanomaterials including aerosol nanoparticles, nanostructured thin films, nanocomposites, CNTs and colloidal nanoparticles, to mention a few. The versatility of microplasma-based systems is especially impressive considering that the first report dates back to only 2002. This is one of the apparent strengths of microplasma technology—a simple, inexpensive and compact system can be used for a large number of applications. While most of the recent reports have focused on small-scale synthesis, scale-up to manufacturing levels is also on the horizon where the features of microplasma-based systems are truly attractive (e.g. atmospheric operation, continuous, portable, etc)

Despite the potential that microplasmas hold for nanomaterials synthesis, some challenges remain. It is clear

that a basic understanding of microplasmas, in terms of both plasma physics and reaction kinetics, is still lacking. Although there are some similarities with low-pressure plasmas, the high operating pressures and resulting modification to the energy exchange mechanisms cannot be neglected. Future efforts in modelling and simulation must include these effects. More importantly for applications, these studies must be connected to microplasma synthesis where chemically reactive gases, solid metal precursors and liquids are used to produce desired materials. Thus, the scientific problems to be resolved are multidimensional and require a synergistic effort that links physics, diagnostics and process.

Acknowledgments

RMS thanks the Case School of Engineering and the NSF Career Award Program (CBET-0746821) for funding support. DM would like to thank Andrew Wagner (University of Minnesota, USA) and Daiji Kawamura (Rochester Institute of Technology, USA). DM also thanks Professor Maguire (University of Ulster, UK) for useful discussions and support.

References

[1] See Becker K H, Schoenbach K H and Eden J G 2006 *J. Phys. D: Appl. Phys.* **39** R55 and references therein
[2] Park S-J and Eden J G 2002 *Appl. Phys. Lett.* **81** 4127
[3] Kurunczi P, Abramzon N, Figus M and Becker K 2004 *Acta Phys. Slovaca* **54** 115
[4] Penache C, Miclea M, Brauning-Demian A, Hohn O, Schossler S, Jahnke T, Niemax K and Schmidt-Bocking H 2002 *Plasma Sources Sci. Technol.* **11** 476
[5] Iza F, Lee J K and Kong M G 2007 *Phys. Rev. Lett.* **99** 075004
[6] El-Habachi A and Schoenbach K H 1998 *Appl. Phys. Lett.* **73** 885
[7] Sankaran R M, Giapis K P, Moselhy M and Schoenbach K H 2003 *Appl. Phys. Lett.* **83** 4728
[8] Park S-H, Eden J G, Chen J and Liu C 2004 *Appl. Phys. Lett.* **85** 4869
[9] Wagner A J, Mariotti D, Yurchenko K J and Das T K 2009 *Phys. Rev.* E **80** 065401(R)
[10] See Karanassios V 2004 *Spectrochim. Acta* B **59** 909 and references therein
[11] Schutze A, Jeong J Y, Babayan S E, Park J, Selwyn G S and Hicks R F 1998 *IEEE Trans. Plasma Sci.* **26** 1685
[12] Sankaran R M and Giapis K P 2001 *Appl. Phys. Lett.* **79** 593
[13] Wilson C G and Gianchandani Y B 2001 *J. Microelectromech. Syst.* **10** 50
[14] Yoshiki H, Ikeda K, Wakaki A, Togashi S, Taniguchi K and Horiike Y 2003 *Japan. J. Appl. Phys. Part 1* **42** 4000
[15] Ichiki T, Taura R and Horiike Y 2004 *J. Appl. Phys.* **95** 35
[16] Okumura T, Saitoh M and Matsuda I 2004 *Japan. J. Appl. Phys. Part 1* **43** 3959
[17] Ideno T and Ichiki T 2004 *J. Photopolym. Sci. Technol.* **17** 173
[18] Tan H, Ideno T and Ichiki T 2005 *J. Photopolym. Sci. Technol.* **18** 237
[19] Chai J, Li B and Kwok D Y 2005 *Appl. Phys. Lett.* **86** 034107
[20] Chiang W, Cochey M, Craig Virnelson R and Sankaran R M 2007 *Appl. Phys. Lett.* **91** 021501
[21] West J, Michels A, Kittel S, Jacob P and Franzke J 2007 *Lab Chip* **7** 981
[22] Vogelsang A, Ohl A, Steffen H, Foest R, Schroder K and Weltmann K-D 2010 *Plasma Process. Polym.* **7** 16
[23] Ito T, Izaki T and Terashima K 2001 *Thin Solid Films* **386** 300
[24] Sankaran R M and Giapis K P 2002 *J. Appl. Phys.* **92** 2406
[25] Sankaran R M and Giapis K P 2003 *J. Phys. D: Appl. Phys.* **36** 2914
[26] Butyagin P I, Khokhryakov Ye V and Mamaev A I 2003 *Mater. Lett.* **57** 1748
[27] Kikuchi T, Hasegawa Y and Shirai H 2004 *J. Phys. D: Appl. Phys.* **37** 1537
[28] Sakurai Y, Kobayashi T, Hasegawa Y and Shirai H 2005 *Japan. J. Appl. Phys. Part 2* **44** 749
[29] Benedikt J, Focke K, A Yanguas-Gil and A von Keudell 2006 *Appl. Phys. Lett.* **89** 251504
[30] Benedikt J, Raballand V, Yanguas-Gil A, Focke K and von Keudall A 2007 *Plasma Phys. Control. Fusion* **49** B419
[31] Yao Z, Jiang Z, Wang F and Xue W 2007 *Appl. Surf. Sci.* **253** 4267
[32] Wang L, Wang H, Shaochun H and Cao X 2007 *Plasma Sci. Technol.* **9** 52
[33] Shirai H, Sakurai Y, Yeo M, Haruta K, Kobayashi T and Ishikawa T 2008 *Thin Solid Films* **516** 4456
[34] Raballand V, Benedikt J and von Keudell A 2008 *Appl. Phys. Lett.* **92** 091502
[35] Raballand V, Benedikt J, Hofmann S, Zimmermann M and von Keudall A 2009 *J. Appl. Phys.* **105** 083304
[36] Ding Y and Shirai H 2009 *J. Appl. Phys.* **105** 043515
[37] Ding Y, He D and Shirai H 2009 *J. Phys. D: Appl. Phys.* **42** 125503
[38] Ito T and Terashima K 2001 *Thin Solid Films* **390** 234
[39] Ostrikov K 2005 *Rev. Mod. Phys.* **77** 489
[40] Ostrikov K and Murphy A B 2007 *J. Phys. D: Appl. Phys.* **40** 2223
[41] Kortshagen U 2009 *J. Phys. D: Appl. Phys.* **42** 113001
[42] See Watanabe Y 2006 *J. Phys. D: Appl. Phys.* **39** R329 and references therein
[43] i Cabarrocas P R, Gay P and Hadjadj A 1996 *J. Vac. Sci. Technol.* A **14** 655
[44] Stoffels W W, Stoffels E, Ceccone G and Rossi F 1999 *J. Vac. Sci. Technol.* A **17** 3385
[45] Sankaran R M, Holunga D, Flagan R C and Giapis K P 2005 *Nano Lett.* **5** 537
[46] Wagner J and Kohler J M 2005 *Nano Lett.* **5** 685
[47] Mariotti D, Svrcek V and Kim D-G 2007 *Appl. Phys. Lett.* **91** 183111
[48] Arnoult G, Belmonte T and Henrion G 2010 *Appl. Phys. Lett.* **96** 101505
[49] Couchman P R and Jesser W A 1977 *Nature* **269** 481
[50] Eden J G and Park S-J 2005 *Plasma Phys. Control. Fusion* **47** B83
[51] Foest R, Schmidt M and Becker K 2006 *Int. J. Mass Spectrom.* **248** 87
[52] Tachibana K 2006 *IEEJ Trans.* **1** 145
[53] Iza F, Kim G J, Lee S M, Lee J K, Walsh J L, Zhang Y T and Kong M G 2008 *Plasma Process. Polym.* **5** 322
[54] Eden J G and Park S-J 2006 *Phys. Plasmas* **13** 057101
[55] Kanazawa S, Daidai R, Akamine S and Ohkubo T 2008 *Surf. Coat. Technol.* **202** 5275
[56] Bryant P M, Szili E J, Whittle T, Park S-J, Eden J G, Al-Bataineh S, Steele D A, Short R D and Bradley J W 2010 *Surf. Coat. Technol.* **204** 2279
[57] Ellerweg D, Benedikt J, von Keudell A, Knake N and Schulz-von der Gathen V 2010 *New J. Phys.* **12** 013021
[58] Kushner M J 2005 *J. Phys. D: Appl. Phys.* **38** 1633
[59] Lee D-S, Sakai O and Tachibana K 2009 *Japan. J. Appl. Phys. Part 1* **48** 106002
[60] Mariotti D and Ostrikov K 2009 *J. Phys. D: Appl. Phys.* **42** 092002
[61] Moselhy M, Petzenhauser I, Frank K and Schoenbach K H 2003 *J. Phys. D: Appl. Phys.* **36** 2922
[62] Rosenberg M 2010 *IEEE Trans. Plasma Sci.* **38** 1
[63] Mariotti D 2008 *Appl. Phys. Lett.* **92** 151505

[64] Raizer Y P 1991 *Gas Discharge Physics* 2nd edn (Berlin: Springer)
[65] Staack D, Farouk B, Gutsol A and Fridman A 2005 *Plasma Sources Sci. Technol.* **14** 700
[66] Staack D, Farouk B, Gutsol A and Fridman A 2008 *Plasma Sources Sci. Technol.* **17** 025013
[67] Benedikt J 2010 *J. Phys. D: Appl. Phys.* **43** 043001
[68] Chantry P J 1987 *J. Appl. Phys.* **62** 1141
[69] Choi J, Iza F and Lee J K 2007 *IEEE Trans. Plasma Sci.* **35** 1274
[70] Wilson C G, Gianchandani Y B, Arslanbekov R R and Kolobov V 2003 *J. Appl. Phys.* **94** 2845
[71] Mariotti D, Shimizu Y, Sasaki T and Koshizaki N 2006 *Appl. Phys. Lett.* **89** 201502
[72] Liu D W, Iza F and Kong M G 2009 *Appl. Phys. Lett.* **95** 031501
[73] Li B, Chen Q and Liu Z W 2010 *Appl. Phys. Lett.* **96** 041502
[74] Lu X, Jiang Z, Xiong Z, Tang Z and Pan Y 2008 *Appl. Phys. Lett.* **92** 151504
[75] Park J, Henins I, Herrmann H W and Selwyn G S 2001 *J. Appl. Phys.* **89** 15
[76] Elenbaas W 1951 *The High Pressure Mercury Vapor Discharge* (Amsterdam: North-Holland)
[77] Tomai T, Kikuchi H, Nakahara S, Yui H and Terashima K 2008 *Trans. Mater. Res. Soc. Japan* **33** 355
[78] Mariotti D, Shimizu Y, Sasaki T and Koshizaki N 2007 *J. Appl. Phys.* **101** 013307
[79] Farouk T, Farouk B and Fridman A 2010 *IEEE Trans. Plasma Sci.* **38** 73
[80] Petrovic Z L, Skoro N, Maric D, Mahony C M O, Maguire P D, Radmilovic-Radenovic M and Malovic G 2008 *J. Phys. D: Appl. Phys.* **41** 194002
[81] Go D B, Fisher T S, Garimella S V and Bahadur V 2009 *Plasma Sources. Sci. Technol.* **18** 035004
[82] Belostotskiy S G, Ouk T, Donnelly V M, Economou D J and Sadeghi N 2010 *J. Appl. Phys.* **107** 053305
[83] Sawada M, Tomai T, Ito T, Fujiwara H and Terashima K 2006 *J. Appl. Phys.* **100** 123304
[84] Petrovic Z L, Malovic G, Radmilovic-Radjenovic M, Puac N, Maric D, Maguire P and Mahony C 2006 *Proc. 25th Int. Conf. Microelectronics (Belgrade, 14–17 May 2006)*
[85] Mariotti D, McLaughlin J A and Maguire P 2004 *Plasma Sources Sci. Technol.* **13** 207
[86] Go D B and Pohlman D A 2010 *J. Appl. Phys.* **107** 103303
[87] Park J, Henins I, Herrmann H W and Selwyn G S 2001 *J. Appl. Phys.* **89** 20
[88] Shi J J and Kong M G 2006 *Phys. Rev. Lett.* **96** 105009
[89] Laux C O, Spence T G, Kruger C H and Zare R N 2003 *Plasma Sources Sci. Technol.* **12** 125
[90] Narendra J J, Grotjohn T A and Asmussen J 2008 *Plasma Sources Sci. Technol.* **17** 035027
[91] Schulz-von der Gathen V, Schaper L, Knake N, Reuter S, Niemi K, Gans T and Winter J 2008 *J. Phys. D: Appl. Phys.* **41** 194004
[92] Knake N, Reuter S, Niemi K, Schulz-von der Gathen V and Winter J 2008 *J. Phys. D: Appl. Phys.* **41** 194006
[93] Knake N, Niemi K, Reuter S, V Schulz-von der Gathen and Winter J 2008 *Appl. Phys. Lett.* **93** 131503
[94] Staack D, Farouk B, Gutsol A F and Fridman A 2007 *IEEE Trans. Plasma Sci.* **35** 1448
[95] Zhu L-G, Chen W-C, Zhu X-M, Pu Y-K and Li Z-R 2009 *Rev. Sci. Instrum.* **80** 023105
[96] Choi J-Y, Takano N, Urabe K and Tachibana K 2009 *Plasma Sources Sci. Technol.* **18** 035013
[97] Sakai O, Sakaguchi T, Ito Y and Tachibana K 2005 *Plasma Phys. Control. Fusion* **47** B617
[98] Belostotskiy S G, Khandelwal R, Wang Q, Donnelly V M, Economou D J and Sadeghi N 2008 *Appl. Phys. Lett.* **92** 221507
[99] Ito Y, Sakai O and Tachibana K 2010 *Plasma Sources Sci. Technol.* **19** 025006
[100] Yanguas-Gil A, Focke K, Benedikt J and von Keudell A 2007 *J. Appl. Phys.* **101** 103307
[101] Ichiki T, Koidesawa T and Horiike Y 2003 *Plasma Sources Sci. Technol.* **12** S16
[102] Zhu X-M, Chen W-C and Pu Y-K 2008 *J. Phys. D: Appl. Phys.* **41** 105212
[103] Ogata K and Terashima K 2009 *J. Appl. Phys.* **106** 023301
[104] Sismanoglu B N, Amorim J, Souza-Correa J A, Oliveira C and Gomes M P 2009 *Spectrochim. Acta Part B* **64** 1287
[105] Stauss S, Imanishi Y, Miyazoe H and Terashima K 2010 *J. Phys. D: Appl. Phys.* **43** 155203
[106] Hong Y C and Uhm H S 2006 *Appl. Phys. Lett.* **89** 221504
[107] Belostotskiy S G, Donnelly V M and Economou D J 2008 *Plasma Sources Sci. Technol.* **17** 045018
[108] Rao N, Girschick S, Heberlein J, McMurry P, Jones S, Hansen D and Micheel B 1995 *Plasma Chem. Plasma Process.* **15** 581
[109] Shimizu Y, Sasaki T, Ito T, Terashima K and Koshizaki N 2003 *J. Phys. D: Appl. Phys.* **36** 2940
[110] Zou Q, Wang M, Li Y and Zou L 2009 *J. Low Temp. Phys.* **157** 557
[111] Chiang W-H and Sankaran R M 2007 *Appl. Phys. Lett.* **91** 121503
[112] Camata R P, Atwater H A, Valhalla K J and Flagan R C 1996 *Appl. Phys. Lett.* **68** 3162
[113] Chiang W-H and Sankaran R M 2008 *Phys J. Chem.* C **112** 17920
[114] Mangolini L, Thimsen E and Kortshagen U 2005 *Nano Lett.* **5** 655
[115] Flagan R C and Lunden M M 1995 *Mater. Sci. Eng.* A **204** 113
[116] Chiang W-H and Sankaran R M 2008 *Adv. Mater.* **20** 4857
[117] Nozaki T, Sasaki K, Ogino T, Asahi D and Okazaki K 2007 *Nanotechnology* **18** 235603
[118] Nozaki T and Okazaki K 2006 *Pure Appl. Chem.* **78** 1157
[119] Kona S, Kim J H, Harnett C K and Sunkara M K 2009 *IEEE Trans. Nanotechnol.* **8** 286
[120] Yoshiki H, Okada T, Hirai K and Hatakeyama R 2006 *Japan. J. Appl. Phys.* **45** 9276
[121] Yoshiki H and Mitsui T 2008 *Surf. Coat. Technol.* **202** 5266
[122] Yoshiki H and Saito T 2008 *J. Vac. Sci. Technol.* A **26** 338
[123] Agiral A, Lefferts L and Gardeniers J G E 2009 *IEEE. Trans. Plasma Sci.* **37** 985
[124] Shimizu Y, Sasaki T, Ito T, Terashima K and Koshizaki N 2003 *J. Phys. D: Appl. Phys.* **36** 2940
[125] Mariotti D, Bose A C and Ostrikov K 2009 *IEEE Trans. Plasma Sci.* **37** 1027
[126] Shimizu Y, Koga K, Sasaki T and Koshizaki N 2009 *Cryst. Eng. Commun.* **11** 1940
[127] Shimizu Y, Bose A C, Sasaki T, Mariotti D, Kirihara K, Kodaira T, Terashima K and Koshizaki N 2006 *Trans. Mater. Res. Soc. Japan* **31** 463
[128] Bose A C, Shimizu Y, Mariotti D, Sasaki T, Terashima K and Koshizaki N 2006 *Nanotechnology* **17** 5976
[129] Shimizu Y, Sasaki T, Liang C, Bose A C, Ito T, Terashima K and Koshizaki N 2005 *Chem. Vapor Depos.* **11** 244
[130] Shimizu Y, Sasaki T, Bose A C, Terashima K and Koshizaki N 2006 *Surf. Coat. Technol.* **200** 4251
[131] Shimizu Y, Kawaguchi K, Sasaki T and Koshizaki N 2009 *Appl. Phys. Lett.* **94** 191504
[132] Shimizu Y, Koga K, Sasaki T, Mariotti D, Terashima K and Koshizaki N 2007 *Microprocess. Nanotechnol. 2007, Digest of Papers* 174
[133] Shimizu Y, Bose A C, Mariotti D, Sasaki T, Kirihara K, Suzuki T, Terashima K and Koshizaki N 2006 *Japan. J. Appl. Phys. Part 1* **45** 8228

[134] Mariotti D, Lindstrom H, Bose A C and Ostrikov K 2008 *Nanotechnology* **19** 495302
[135] Ito T and Terashima K 2002 *Appl. Phys. Lett.* **80** 2648
[136] Cvelbar U, Ostikov K and Mozetic M 2008 *Nanotechnology* **19** 405605
[137] Wolter M, Levchenko I, Kersten H and Ostrikov K 2010 *Appl. Phys. Lett.* **96** 133105
[138] Shirai H, Kobayashi T and Hasegawa Y 2005 *Appl. Phys. Lett.* **87** 143112
[139] Yang Z, Kikuchi T, Hatou Y, Kobayashi T and Shirai H 2005 *Japan. J. Appl. Phys. Part 1* **44** 4122
[140] Yang Z, Shirai H, Kobayashi T and Hasegawa Y 2007 *Thin Solid Films* **515** 4153
[141] Gubkin J 1887 *Ann. Phys.* **32** 114
[142] Denaro A R and Hickling A 1958 *J. Electrochem. Soc.* **105** 265
[143] Hickling A and Ingram M D 1964 *J. Electroanal. Chem.* **8** 65
[144] Harada K and Iwasaki T 1974 *Nature* **250** 426
[145] Harada K and Suzuki S 1977 *Nature* **266** 275
[146] Sano N, Wang H, Chhowalla M, Alexandrou I and Amaratunga G A J 2001 *Nature* **414** 506
[147] Baba K, Kaneko T and Hatakeyama R 2007 *Appl. Phys. Lett.* **90** 201501
[148] Yamatake A, Fletcher J, Yasuoka K and Ishii S 2006 *IEEE Trans. Plasma Sci.* **34** 1375
[149] Sakiyama Y, Tomai T, Miyano M and Graves D B 2009 *Appl. Phys. Lett.* **94** 161501
[150] Fridman G, Brooks A D, Balasubramanian M, Fridman A, Gutsol A, Vasilets V N, Ayan H and Friedman G 2007 *Plasma Process. Polym.* **4** 370
[151] Lee H J, Shon C H, Kim Y S, Kim S, Kim G C and Kong M G 2009 *New J. Phys.* **11** 115026
[152] Jo K-W, Kim M-G, Shin S-M and Lee J-H 2008 *Appl. Phys. Lett.* **92** 011503
[153] Staack D, Fridman A, Gutsol A, Gogotsi Y and Friedman G 2008 *Angew. Chem. Int. Edn* **47** 8020
[154] Okada T, Kaneko T and Hatakeyama R 2007 *Thin Solid Films* **515** 4262
[155] Kaneko T, Okada T and Hatakeyama R 2007 *Contrib. Plasma Phys.* **47** 57
[156] Imasaka K, Kato Y and Suehiro J 2007 *Nanotechnology* **18** 335602
[157] Bhattacharyya S, Staack D, Vitol E A, Singhal R, Fridman A, Friedman G and Gogotsi Y 2009 *Adv. Mater.* **21** 4039
[158] Baba K, Kaneko T and Hatakeyama R 2009 *Appl. Phys. Exp.* **2** 035006
[159] Chen Q, Kitamura T, Saito K, Haruta K, Yamano Y, Ishikawa T and Shirai H 2008 *Thin Solid Films* **516** 4435
[160] Koo I G, Lee M S, Shim J H, Ahn J H and Lee W M 2005 *J. Mater. Chem.* **15** 4125
[161] Furuya K, Hirowatari Y, Ishioka T and Harata A 2007 *Chem. Lett.* **36** 1088
[162] Furusho H, Kitano K, Hamaguchi S and Nagasaki Y 2009 *Chem. Mater.* **21** 3526
[163] Schmid G 1994 *Nanoparticles: From Theory to Applications* (Weinheim: Wiley-VCH)
[164] Hieda J, Saito N and Takai O 2008 *J. Vac. Sci. Technol.* A **26** 854
[165] Shirai N, Nakazawa M, Ibuka S and Ishii S 2009 *Japan. J. Appl. Phys. Part 1* **48** 036002
[166] Richmonds C M and Sankaran R M 2008 *Appl. Phys. Lett.* **93** 131501
[167] Chiang W-H, Richmonds C and Sankaran R M 2010 *Plasma Sources Sci. Technol.* **19** 034011
[168] Chang F-C, Richmonds C and Sankaran R M 2010 *J. Vac. Sci. Technol.* A **28** L5
[169] Meiss S A, Rohnke M, Kienle L, El Abedin S Z, Endres F and Janek J 2007 *Chem. Phys. Chem.* **8** 50
[170] Zou J-J, Zhang Y-P and Liu C-H 2006 *Langmuir* **22** 11388
[171] Tomai T, Katahira K, Kubo H, Shimizu Y, Sasaki T, Koshizaki N and Terashima K 2007 *J. Supercrit. Fluids* **41** 404
[172] Noma Y, Choi J H, Tomai T and Terashima K 2008 *Appl. Phys. Lett.* **93** 101503
[173] Levchenko I, Ostrikov K and Mariotti D 2008 *Carbon* **47** 344
[174] Levchenko I, Ostrikov K, Mariotti D and Svrcek V 2009 *Carbon* **47** 2379
[175] Nunomura S, Kita M, Koga K, Shiratani M and Watanabe Y 2006 *J. Appl. Phys.* **99** 083302
[176] Nunomura S, Yoshida I and Kondo M 2009 *Appl. Phys. Lett.* **94** 071502
[177] Švrček V, Kondo M, Kalia K and Mariotti D 2009 *Chem. Phys. Lett.* **478** 224
[178] Švrček V, Fujiwara H and Kondo M 2009 *Acta Mater.* **57** 5986
[179] Švrček V, Mariotti D and Kondo M 2009 *Opt. Exp.* **17** 520
[180] Švrček V and Kondo M 2009 *Appl. Surf. Sci.* **255** 9643
[181] Chiang W-H and Sankaran R M 2009 *Nature Mater.* **8** 882
[182] Chiang W-H, Sakr M, Gao X P A and Sankaran R M 2009 *ACS Nano* **3** 4023
[183] Sakai O, Naito T, Shimomura T and Tachibana K 2010 *Thin Solid Films* **518** 3444
[184] Koretzky E and Kuo S P 1998 *Phys. Plasma* **5** 3774
[185] Cao Z, Walsh J L and Kong M G 2009 *Appl. Phys. Lett.* **94** 021501
[186] Cao Z, Nie Q, Bayliss D L, Walsh J L, Ren C S, Wang D Z and Kong M G 2010 *Plasma Sources. Sci. Technol.* **19** 025003
[187] Kong M G, Kroesen G, Morfill G, Nosenko T, Shimizu T, van Dijk J and Zimmermann J L 2009 *New. J. Phys.* **11** 115012
[188] Heberlein J and Murphys A B 2008 *J. Phys. D: Appl. Phys.* **41** 053001
[189] Shimizu K, Sugiyama T, Nishamani M and Kanamori M 2009 *IEEE Trans. Indust. Appl.* **45** 1506
[190] Boettner H, Waskoenig J, O'Connell D, Kim T L, Tchertchian P A, Winter J and Schulz-von der Gathen V 2010 *J. Phys. D: Appl. Phys.* **43** 124010
[191] Meng L G, Liu C L, Liang H F and Liang Z H 2008 *Phys. Lett.* A **372** 6504
[192] Eden J G, Park S-J and Kim K-S 2006 *Plasma Sources Sci. Technol.* **15** S67
[193] Zissis G and Kitsinelis S 2009 *J. Phys. D: Appl. Phys.* **42** 173001
[194] Nie Q Y, Cao Z, Ren C S, Wang D Z and Kong M G 2009 *New. J. Phys.* **11** 115015